



ELSEVIER

Contents lists available at ScienceDirect

Regulatory Toxicology and Pharmacology

journal homepage: www.elsevier.com

Transcriptional profiling of male CD-1 mouse lungs and harderian glands supports the involvement of calcium signaling in acrylamide-induced tumors

Nikolai L. Chepelev^{a, b}, Rémi Gagné^b, Timothy Maynor^a, Byron Kuo^b, Cheryl A. Hobbs^a, Leslie Recio^a, Carole L. Yauk^{b, *}

^a Integrated Laboratory Systems Inc., Research Triangle Park, NC 27709, USA

^b Environmental Health Science and Research Bureau, Environmental and Radiation Health Sciences Directorate, HECSB, Health Canada, Ottawa, ON K1A 0K9, Canada

ARTICLE INFO

Keywords:

Human health risk assessment
Mode of action
Lung
Harderian gland
Gene expression
Calcium signaling
Dose-response

ABSTRACT

Acrylamide (AA) exposure causes increased incidence of forestomach, lung, and Harderian gland tumors in male mice. One hypothesized mode of action (MOA) for AA-carcinogenicity includes genotoxicity/mutagenicity as a key event, possibly resulting from AA metabolism to the direct genotoxic metabolite glycidamide. Alternatively, altered calcium signaling (CS) has been proposed as a central key event in the MOA. To examine the plausibility of these proposed MOAs, RNA-sequencing was performed on tumor target tissues: Harderian glands (the most sensitive tumor target tissue in the rodent 2-year cancer bioassay) and lungs of AA-exposed male CD-1 mice. Animals were exposed to 0.0, 1.5, 3.0, 6.0, 12.0, or 24.0 mg AA/kg bw-day in drinking water for 5, 15, or 31 days. We observed a pronounced effect on genes involved in CS and cytoskeletal processes in both tissues, but no evidence supporting a genotoxic MOA. Benchmark dose modeling suggests transcriptional points of departure (PODs) of 0.54 and 2.21 mg/kg bw-day for the Harderian glands and lungs, respectively. These are concordant with PODs of 0.17 and 1.27 mg/kg bw-day derived from the cancer bioassay data for these tissues in male mice, respectively. Overall, this study supports the involvement of CS in AA-induced mouse carcinogenicity, which is consistent with a recently proposed CS-based MOA in rat thyroid, and with other published reports of aberrant CS in malignant tumors in rodents and humans.

1. Introduction

Acrylamide (AA) is a well-established human and rodent neurotoxin and a widely-used industrial commodity chemical in polymer manufacturing. It is also found in many foods, especially those with high starch content that are cooked at high temperatures (e.g., French fries). In addition, AA polymers are widely used for many industrial applications, such as a flocculant for clarifying drinking water, as reviewed in (FAO/WHO Joint FAO/WHO Expert Committee on Food Additives, 2011). AA is considered a prototypic neurotoxin that causes distal axonopathy characterized by degeneration of nerve terminal endings (LoPachin and Gavin, 2012). The molecular mechanisms related to AA neurotoxicity may include its binding to neurofilament and microtubule proteins in rat spinal cord, as demonstrated decades previously (Lapadula et al., 1989; Reagan et al., 1994). In addition, more recent proteomic evidence (LoPachin and Gavin, 2012) illustrates the electrophilic potential

of AA to bind to cysteine thiolate groups of presynaptic proteins and proteins involved in axonal transport. This leads to aberrant nerve terminal processes at high AA exposures, producing a characteristic axonal neuropathy in humans and rodents (LoPachin and Gavin, 2012).

The binding of AA to motor proteins involved in axonal transport is speculated as the basis for not only AA neurotoxicity (Sickles et al., 2002), but also for the genotoxic effects of AA (Friedman et al., 2008). Both neurotoxicity and cancer endpoints have been used to calculate reference doses for AA for regulatory evaluation (Shipp et al., 2006). These reference doses are very similar (1.2 and 1.5 mg/kg bw-day, for neurotoxicity and carcinogenicity, respectively) (Shipp et al., 2006). A more recent comparison (EFSA Panel on Contaminants in the Food Chain (CONTAM), 2015) also gives similar BMDLs (the lower 95% confidence interval on the benchmark dose) for both carcinogenicity (0.17 mg/kg bw-day, based on incidence of Harderian gland adenoma in male mice in a two-year cancer bioassay) and neurotoxicity (0.43 mg/kg bw-day, based on incidence of peripheral nerve (sciatic)

* Corresponding author. Environmental Health Centre, Tunney's Pasture Bldg. 8 (P/L 0803A), 50 Colombine Driveway, Ottawa, Ontario K1A 0K9, Canada.
Email address: carole.yauk@canada.ca (C.L. Yauk)

axonal degeneration in male F344 rats exposed to AA in drinking water daily, for two years). The fact that AA induces both neurotoxicity and carcinogenicity at similar doses led us to question whether the two toxicities are mechanistically related, as we recently proposed for benzo[a]pyrene (Chepelev et al., 2015a,b). Identifying an interconnection between these toxicological effects would enable us to mine the molecular neurotoxicity data for further insight into mechanisms involved in AA-induced cancer.

AA-induced carcinogenicity has been shown in all of the four 2-year cancer bioassays conducted to date (Johnson et al., 1986; Friedman et al., 1995; Beland et al., 2013; Maronpot et al., 2015). All four bioassays showed increased incidence of thyroid tumors in rats. In Fisher rats, but not Han Wistar rats, AA also produced tunica vaginalis mesotheliomas. In mice, tumors were detected in the Harderian gland, lung, and forestomach of both sexes (Beland et al., 2013). Harderian gland is the most sensitive target organ of AA-induced carcinogenicity identified to date from the four cancer bioassays conducted. Although humans lack Harderian glands (Albert et al., 1986), this gland is a sensitive target tissue to detect compounds that are both genotoxic and carcinogenic in rodents. Therefore, the Harderian gland is considered to be “a conservative endpoint for assessment of the risk for neoplastic effects of AA in humans” and the data on the incidence of Harderian gland tumors in male mice have been used to derive a “reference point” or “point of departure” (POD) by some international agencies (EFSA Panel on Contaminants in the Food Chain (CONTAM), 2015).

Unlike AA-mediated neurotoxicity, the mode of action (MOA) of AA-induced carcinogenicity (described in Fig. 1) is poorly understood. While the weight of evidence suggests that AA is “clearly genotoxic in somatic and germ cells” *in vivo* [reviewed in (EFSA Panel on Contaminants in the Food Chain (CONTAM), 2015)], the relevance of

genotoxic properties of AA to cancer endpoints that are observed in animals is enigmatic because covalent adducts of AA with DNA have not been observed *in vitro* or *in vivo*, while glycidamide (GA, a reactive metabolite of AA) is thought to be primarily, if not exclusively, responsible for the formation of DNA adducts in animals dosed with AA [reviewed in (EFSA Panel on Contaminants in the Food Chain (CONTAM), 2015)]. The genotoxic effects of AA appear to arise due to its metabolism by cytochrome P450 family 2, subfamily e, polypeptide 1 enzyme (Cyp2e1) to GA (Ghanayem et al., 2005a, 2005b; Martins et al., 2007; Maronpot et al., 2015); genotoxicity is apparent at high concentrations and shows a sublinear response in cultured mouse cells and in rats (Mei et al., 2008; Dobrovolsky et al., 2016; Hobbs et al., 2016), mice (Zeiger et al., 2009), and rats (Watzek et al., 2012). More specifically, a single-dose oral exposure of female Sprague-Dawley rats to 0.1–10 000 µg AA/kg bw revealed the lack of linearity in the formation of the N7-GA-Gua adducts in the liver, kidney, and lung (Watzek et al., 2012). This result is consistent with the apparent threshold of 1–2 mg/kg bw-day for the N7-GA-Gua adducts in the peripheral red blood cells of male B6C3F1 mice, following 28-day dosing in drinking water (Zeiger et al., 2009). We previously found that male mice treated for 30 days with up to 24.0 mg/kg-bw exhibit no increase in *Pig-a* gene mutations (Hobbs et al., 2016). In the same study, an increase in micronuclei in peripheral blood was observed in mice but not rats (Hobbs et al., 2016). While the presence of such sublinear or “threshold” genotoxic response supports that AA is genotoxic at high doses, it also suggests that genotoxicity is not a key event (KE) in the MOA of AA-induced carcinogenicity (as the doses required to induce genotoxic effects are higher than those causing cancer). This highlights the need to both carefully evaluate the weight-of-evidence supporting the role of genotoxicity in AA's carcinogenicity, and to explore alternative MOAs in AA-induced carcinogenicity in rodents.

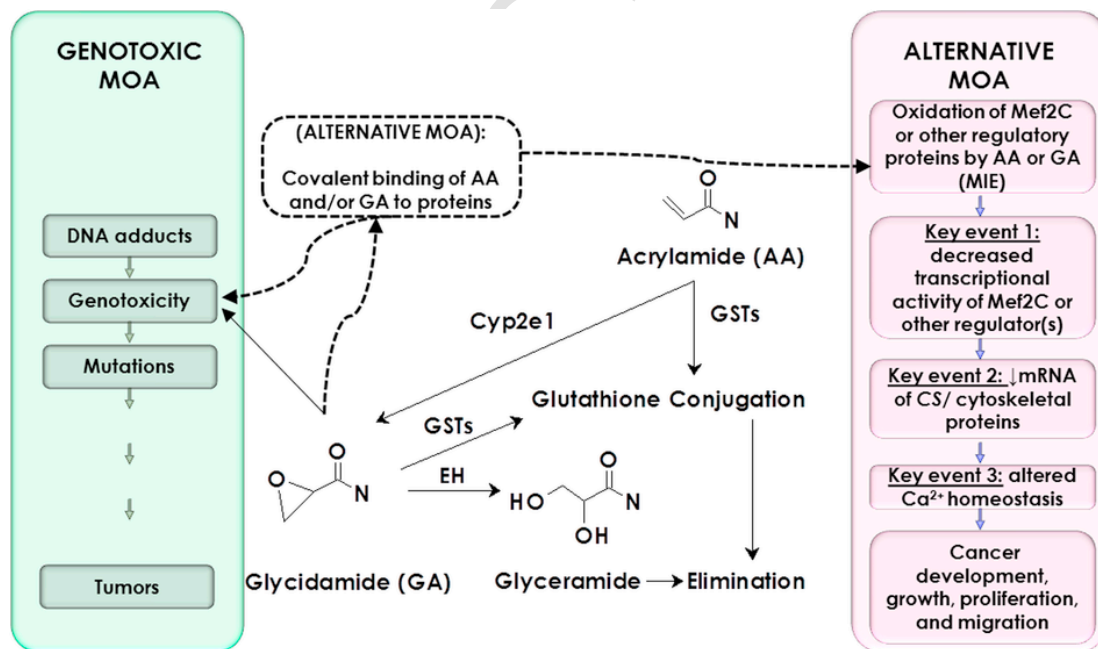


Fig. 1. Proposed genotoxic and CS MOAs of AA-induced lung tumors in male mice. The genotoxic MOA involves AA metabolism to its genotoxic metabolite GA by cytochrome P450 family 2, subfamily e, polypeptide 1 enzyme (Cyp2e1). GA forms adducts with DNA, leading to genotoxicity, mutations, and lung tumors. Alternatively, AA has been proposed to lead to genotoxicity indirectly as a result of covalent binding to cytoskeletal proteins, including microtubules and microfilaments proteins [e.g. (Sickles et al., 2007),]; this mechanism has not been firmly established (dashed arrow). Since toxicokinetic analyses show that oral administration of AA leads to similar AUCs (areas under the time-serum concentration curves from zero to infinity) for AA and GA in plasma in mice and rats, with similar AA and GA levels present in several tissues (Doerge et al., 2005a, 2005b), and since both AA and GA adducts with proteins are well-documented [e.g.(Fennell et al., 2015),], the formation of the AA- and/or GA-protein adducts may be a molecular initiating event (MIE). Epoxide hydrolase (EH) can further metabolize AA to glyceramide (GA). Both AA and GA can be conjugated to glutathione (GSH) by GSH transferases (GSTs). An alternative, calcium signaling- (CS-) based MOA has been proposed based on toxicogenomic profiling of the thyroid glands and livers of male rats exposed to AA (Chepelev et al., 2017). In this MOA, the oxidation of redox-sensitive Cys residues on a key regulatory protein, such as transcription factor Mef2C (MIE), leads to the loss of its function (KE1). Since CS is linked to several cancer hallmarks (Stewart et al., 2015), altered Ca²⁺ homeostasis (KE3) resulting from downregulation of CS genes (KE2) could promote the development, growth, proliferation, and migration of cancer cells, as reviewed in (Hoth, 2016).

Additional alternative MOAs have been considered [e.g. (Eckert, 1985; Sager, 1989; Lapadula et al., 1989; Gall et al., 1992; Sickles et al., 1995, 1996, 2002, 2007; Arocena, 2006; 2007),], some of which involve direct interactions of AA with cytoskeletal proteins including certain kinesins (Sickles et al., 2007) and components of intermediate filaments, vimentin, and keratin (Durham et al., 1983; Eckert, 1985; Gall et al., 1992). While these interactions with structural proteins are thought to contribute to the neurotoxic effects of AA, these have also been suggested to mediate genotoxicity (Friedman et al., 2008). Our recent toxicogenomic studies on F344 male rats exposed to AA daily for up to 30 days provided support for this hypothesis through RNA-sequencing (RNA-seq) of the testes (Recio et al., 2017), livers, and thyroid glands (Chepelev et al., 2017) of AA-exposed and control rats. AA-exposed cancer target tissues (testes and thyroid) showed altered expression in many genes that are part of the cytoskeleton and participate in actin signaling and calcium signaling (CS) including: actins and myosins (*Acta1*, *Myh1*, and *My11*), troponins (*Tnnc2*, *Tnni2*, and *Tnnt3*), and Ryanodine receptor 1 (*Ryr1*); whereas, CS was generally not affected in the non-target tissue (liver). Therefore, we hypothesized that CS perturbation is a plausible KE for AA-induced carcinogenicity in male rats (hypothetical MOA in Fig. 1), but indicated a need for further work to test this hypothesis, which was partially carried out in the present study.

In this study, global transcriptional analysis of mouse target tissues was undertaken to complement our previous rat study and enhance MOA understanding of AA-induced carcinogenicity in rodents. We applied RNA-seq to measure the dose-response of transcriptional changes occurring over time in the lung and Harderian gland tissues of male mice following sub-chronic oral exposure to a wide range of AA doses. Our goals were: i) to examine the temporal- and dose-response concordance of the transcriptional data in support of genotoxicity as a KE, or alternatively, CS as a KE, in the MOA for AA-induced carcinogenicity in mice (referred to as the genotoxicity and CS MOA analyses, respectively); ii) to perform dose-response modeling of apical (cancer) data as a part of a weight of evidence analysis to compare it to toxicogenomic data, thus assessing the plausibility of the genotoxicity vs. CS-based MOA; and iii) to explore the suitability of using a toxicogenomic rather than an apical (cancer) endpoint to derive a POD for potential use in human health risk assessment of AA.

2. Materials and methods

2.1. Animal treatments

Animal treatment procedures were approved by the ILS, Inc. Institutional Animal Care and Use Committee, were in compliance with the Animal Welfare Act Regulations, 9 CFR 1–4, and the Guide for the Care and Use of Laboratory Animals (Institute for Laboratory Animal Research, 1996), and were carried out in an Association for Assessment and Accreditation of Laboratory Animal Care (AAALAC) accredited facility (AAALAC International File number: 000810). Male CD-1 mice were from Charles River Laboratories (Raleigh, NC USA) used because positive genetic toxicity studies (Katen et al., 2016) were reported from this strain in germ cells, suggesting that AA is efficiently metabolized in CD-1 mice. Animals were acclimatized for 8 days and were 8 weeks of age at the onset of the experiment. Animals were on 12/12h light/dark cycle (lights on: off, 0800:2000). They were housed one per cage in polycarbonate cages with micro-isolator tops and were fed NIH-07 Irradiated Open Formula diet (Harlan Teklad Diet, Madison, WI) *ad libitum*. Seven mice were assigned to each dose group using a procedure that stratifies animals across groups by body weight, such that mean body weight of each group was not statistically different from any other group using analysis of variance (ANOVA) (Statistical Analysis System version 9.2, SAS Institute, Cary, NC). AA (CAS No. 79-06-1,

Sigma-Aldrich (St. Louis, MO), batch BCBN4988V) exposure was by *ad libitum* in drinking water (reverse osmosis treated tap water [City of Durham, NC]). AA was prepared weekly in drinking water, and concentrations were adjusted weekly based upon the previous week's group mean body weight and water consumption data.

Drinking water exposures were used to be consistent with previous rodent cancer bioassays. Doses were selected based on our previous report of micronucleus induction by AA in male mice that employed AA up to 24 mg/kg bw-day (Zeiger et al., 2009). Mice were dosed with 0.0, 1.5, 3.0, 6.0, 12, or 24 mg AA/kg bw-day in drinking water. On Days 5, 15, or 31, animals were humanely euthanized by carbon dioxide asphyxiation and death was confirmed by exsanguination. The necropsies were conducted in the morning, over an approximately 4-h period, using one animal per treatment group in sequence (to account for any potential time effect), repeated until all animals were euthanized. The right lobes of the lungs were insufflated in RNAlater® (Qiagen Valencia, CA), cubed, then flash frozen in liquid nitrogen. The Harderian glands were collected and flash frozen in liquid nitrogen. In addition, peripheral blood was collected, over the same time of the day for each time point to control for potential diurnal variation, for analyses of serum hormone levels (Triiodothyronine (T3), Thyroxine (T4), Thyroid Stimulating Hormone [TSH]), as well as Luteinizing Hormone (LH), Prolactin, and Testosterone.

2.2. Ion Proton™ sequencing (RNA-seq)

RNA-seq analysis on the lungs was done using an Ion Proton sequencer. RNA-sequencing for Harderian gland was done on an Illumina NextSeq (described below). Two different platforms were employed concurrently to generate the data in a timely fashion (i.e., different technologies were available in the two laboratories), with the premise that toxicogenomic data should provide insight into the carcinogenic MOA of AA regardless of the platform used. Six biological replicates (randomly selected from the seven animals per dose group) were used per dose group (including controls) at each time point. Frozen lung samples were homogenized in 2-min intervals using 7.0mm stainless steel beads and a Retsch Mixer Mill MM 400 (Verder Scientific, Newtown, PA) at 20Hz, until complete homogenization (no visible tissue) was achieved. Total RNA was isolated from homogenized samples using Qiagen miRNeasy Mini Kits (Qiagen, Valencia, CA) according to the manufacturer's protocol, including on-column DNase I digestion with the RNase-free DNase Set (Qiagen). RNA quantity and A260/280 ratios were measured using a Nanodrop ND-1000 Spectrophotometer (Thermo Fisher Scientific, Waltham, MA). RNA quality was assessed using an Agilent RNA 6000 Nano kit and an Agilent 2100 Bioanalyzer according to the manufacturer's protocol (Agilent Technologies, Santa Clara, CA). The RNA Integrity Numbers (RIN) were generated using the 2100 Expert software (Agilent). Only samples with RINs >7.0 were used for further steps.

Poly-A RNA enrichment was performed on 1.5µg of total RNA using DynaBeads® mRNA DIRECT Micro Kits (Life Technologies, Carlsbad, CA), using up to 96 samples with individual barcodes. Following RNase III fragmentation cDNA library preparation was carried out using Ion Total RNA-seq Kits v2 (Life Technologies, Carlsbad, CA). The 3' and barcode adapters from the Ion Xpress™ RNA-seq Barcode 1–96 Automated Library Construction Kit (Life Technologies, Carlsbad, CA) were ligated to the ends of the fragmented libraries such that each PCR product received a unique barcode. Libraries were amplified using the Platinum® PCR SuperMix, High Fidelity (Life Technologies, Carlsbad, CA). Each library was quantified using the Agilent® Tape Station High Sensitivity DNA Screentape and each sample was diluted to 250 pM. The efficiency of this step was verified by checking the consistency of the average size of the cDNA library fragments for each sample on an Agilent DNA Screentape.

Next, aliquots of each library (up to 96 samples simultaneously) were pooled together to a final concentration of 50 pM. Emulsion PCR, enrichment, and chip loading was done on an Ion Chef™ instrument, using Ion P1™ chips (version 3) and Ion PI™ Chef Kits (Life Technologies, Carlsbad, CA). All chips had approximately 70–90% ion sphere particle loading density. Chips were then used in semi-conductor sequencing by the Ion Proton™ sequencer using the Ion Proton™ HI-Q™ Sequencing Kit (Life Technologies, Carlsbad, CA).

The Proton™ Torrent Server version 4.4.3 interpreted the sequencing data and generated FASTQ files for each barcoded sample. Reads were trimmed to remove low quality read prefixes and suffixes, then aligned to the reference genome (Genome reference consortium (GRC) m38v77 (lung) and GRCm38v84 (Harderian) using Star (Dobin et al., 2013) and Bowtie (Langmead and Salzberg, 2012). The different versions of genomes are due to different time of their releases and incorporation into the laboratory's analytical pipeline.

Gene counting was performed with HT-Seq count (<http://www-huber.embl.de/users/anders/HTSeq/doc/count.html>); the “m” parameter was set to “intersection-nonempty” using the Ensembl GTF annotation. The tables of counts were then imported into R, and genes with total counts less than one read per two million reads were eliminated for both tissues.

3. Illumina RNA-seq

Harderian gland samples were homogenized, RNA was extracted, and quality/quantity checked as described above for the lung samples. Harderian gland dual-indexed next-generation sequencing (NGS) libraries were generated from 2.5 µg of total RNA template using the Illumina TruSeq Stranded mRNA Library Prep Kit HT (Illumina, San Diego, CA) according to the manufacturer's protocol. An aliquot of each NGS library was checked for quality and mean fragment size using an Agilent 2100 Bioanalyzer and the Agilent HS DNA kit or the Agilent DNA 1000 kit. NGS libraries were quantified using the KAPA Library Quantification Kit (KAPA Biosystems, Wilmington, MA) for Illumina platforms with a ViiA™7 Real-Time PCR System (Applied Biosystems™ (ABI), Foster City, CA). Briefly, the KAPA kit quantified diluted libraries against a standard curve (20 pM–0.2 fM) using real-time SYBR Green PCR on a ViiA™7 PCR system. The mean fragment size and quantity were used in library normalization calculations. All libraries were normalized to 10 nM and pooled to 4.0 nM in 10 mM Tris pH 8.5 containing 0.1% Tween 20. The pooled libraries were denatured in 0.2 N sodium hydroxide, and then neutralized in 200 mM Tris pH 7.0. The NGS libraries were further diluted in HT1 Buffer (Illumina) to 1.8 pM and loaded into the NextSeq® 500 (Illumina) for sequencing using a HI Output flow cell (Illumina) with single end reads at 75 cycles. The Illumina Base Space Server interpreted the sequencing data and generated FASTQ files for each sample. Reads were then aligned to the reference genome (Genome reference consortium (GRC) GRCm38v84) using Star (Dobin et al., 2013) and Bowtie (Langmead and Salzberg, 2012).

3.1. Data quality check, assembly, alignment, and normalization

For the data on both tissues, three approaches were used to identify potential outliers and exclude them from further analyses. First, the quality of RNA-seq Toolset (QoRTs) (Hartley and Mullikin, 2015) was used to verify the extent of RNA degradation by examining the bias in the 5'-3' gene-body coverage of the reads. Second, multidimensional scaling plots of distances between gene expression profiles (mdsLog2) generated in EdgeR (Robinson et al., 2010) were used to explore the relationship between samples within and across treatment groups. This resulted in the removal of seven and six samples for the lung and Hard-

erian gland data sets (see Results for details), respectively, out of the 108 samples sequenced for both tissues.

Next, the EdgeR package (Robinson et al., 2010) was used for analysis of RNA-seq data, with TMM normalization (Robinson and Oshlack, 2010). The lists of differentially expressed genes (DEGs) were compiled using the GLM function. DEGs were identified as genes with an unadjusted p-value < 0.001 and fold-change > ± 1.5 cut-offs, relative to their time-matched controls. The complete datasets for both tissues are publicly available at the Sequence Read Archive (SRA; <http://www.ncbi.nlm.nih.gov/sra>, project number PRJNA390168).

3.2. Reverse transcription and quantitative real-time polymerase chain reaction (qRT-PCR)

Some DEGs identified from the RNA-seq data that were deemed relevant for the hypothesized cancer MOAs of AA were selected for Real-Time PCR (qRT-PCR) confirmation. Reverse transcription was performed using High Capacity cDNA Reverse Transcription Kits (Applied Biosystems™ (ABI), Foster City, CA), according to the manufacturer's protocol (thermal cycling conditions: 25 °C for 10 min; 37 °C for 120 min; 85 °C for 5 min; and 4 °C hold). The qRT-PCR reactions were amplified using 20 ng of cDNA template, TaqMan® Fast Advanced Master Mix (ABI), and TaqMan® Gene Expression Assays (ABI). The qRT-PCR was performed using a ViiA™ 7 Real-Time PCR System (ABI) with manufacturer recommended thermal cycling conditions for TaqMan® Fast Advanced Master Mix (50 °C for 2 min; 95 °C for 20 s; 95 °C for 1 s, and 60 °C for 20 s for 40 cycles). The mRNA levels were quantified using the cycle threshold (C_T) values and were normalized to *Actβ* expression. *Actβ* showed stable expression in control and AA-treated samples, based on the RNA-seq data (not shown). Descriptive statistics (mean and standard error) were analyzed using Analyse-It® v2.30 (Analyse-It Software, Leeds, UK) with a confidence interval of 95% for the vehicle control group. Data were reported as the Relative Quantification (RQ; where $RQ = 2^{-(\Delta\Delta C_T)}$).

3.3. Bioinformatic analyses

DEGs were uploaded into Ingenuity Pathway Analysis™ (IPA™, Ingenuity Systems, Redwood City, CA) and Illumina's Correlation Engine (formerly known as NextBio™; <http://nextbio.com>) to identify biological processes that were potentially affected by AA exposure. IPA groups genes into “canonical pathways” that are known cellular signaling pathways. The IPA ‘Upstream Analysis’ feature identifies transcriptional regulators that can explain observed gene expression changes in a given dataset. IPA ‘Diseases and Bio Functions’ identifies potential phenotypic consequences of a perturbed pattern of gene expression, based on data curated from published literature. IPA uses a Fisher's exact test to determine the statistical significance of associations. Z-scores derived in IPA were used to identify potential transcriptional activators or canonical pathways that were activated (Z-score > 2.0) or potential transcriptional inhibitors or canonical pathways that were inhibited (Z-score < 2.0). In addition, the “Functional Annotation Tool” of the Database for Annotation, Visualization and Integrated Discovery (DAVID; <https://david.ncifcrf.gov/>), was used to determine functional annotations of the identified DEGs, with DAVID's default settings.

3.4. Benchmark dose (BMD) modeling

Apical data used here were adenoma incidence from the 2-year cancer bioassay (Beland et al., 2013) from male B6C3F1 mice. These were analyzed using the US EPA's BMDS software, version 2.60, with BMDS

Wizard v.1.10 Output Report, available at: <http://www.epa.gov/ncea/bmds/>.

The normalized, log₂-transformed expression data were analyzed using BMDEExpress (version 1.41) (Yang et al., 2007). All of the data were entered into BMDEExpress, but only transcripts that had an ANOVA filter of $p < 0.05$ for treated versus control samples in at least one dose group were modeled. The data were fit as continuous data to Hill, power, linear, and second degree polynomial models, assuming constant variance. The maximum number of iterations was 250, benchmark response (BMR) factor was set to 1.349 (which approximates a 10% response), confidence level was 0.95, and power was restricted to ≥ 1 . A best-fit model was selected based on: (1) a nested chi-square test cut-off of 0.05 to select between linear and polynomial models; (2) the lowest Akaike information criterion value for the Hill and Power models; and (3) a likelihood ratio test for the goodness-of-fit p -value > 0.1 . For the Hill model, the output was flagged if the k parameter was $< 1/3$ of the lowest dose, in which case the next best fit model was selected if it had a goodness-of-fit p -value > 0.05 . If the next best fit model was unavailable, the BMD was reported as half the BMD of the lowest flagged Hill model. The BMD analyzed datasets were mapped to the IPA canonical pathways using the Defined Category Analysis feature of BMDEExpress. Genes with BMD values greater than the highest dose were removed. All genes with BMDs were analyzed in BMDEExpress Data Viewer (Kuo et al., 2015).

4. Results

4.1. General response of mice to AA

Animals exposed to AA for up to 31 days displayed no signs of morbidity and there were no changes in final body weight or organ weight in exposed vs. concurrent controls (data not shown). A statistically significant decrease (Dunnett's test, $p < 0.05$) in final body weight gain was observed in animals administered the two highest doses on day 5 compared to the control group (data not shown). Body weight gain was not significantly different from concurrent controls on day 15 or day 31 (data not shown). There were statistically significant (Dunnett's test, $p < 0.05$) decreases in water consumption in mice exposed to 6.0 and 12 mg/kg bw-day on day 5, and to 1.5, 12, and 24 mg/kg bw-day on day 31, compared to the concurrent controls (data not shown). No significant differences in water consumption were found for the day 15 group. Actual acrylamide exposures were calculated based on the water consumption data and were within 20% of nominal dose levels. Serum hormone levels were not altered consistently or in a dose-responsive manner. Specifically, there were no changes in T4, prolactin, or testosterone levels, but there were sporadic changes in T3 and TSH levels, and some statistically significant increases in LH levels on day 15 only (data not shown).

4.2. Benchmark dose (BMD) analyses of apical data

BMD modeling of the incidence of the three tumor types observed in male mice in the 2-year cancer bioassay (Beland et al., 2013) is shown in Table 1 (best-fit models are shown here; the data for all models are available in Supplementary File S1). BMD models for all four endpoints had acceptable goodness of fit p -values (> 0.1). The BMDL (lower 95% confidence interval estimates on the BMD) of 0.17 mg/kg bw-day for the Harderian gland data is identical to that reported in the literature (EFSA Panel on Contaminants in the Food Chain (CONTAM), 2015). There is an approximate 10-fold spread of the BMDL values, from 0.17 mg/kg bw-day for the incidence of Harderian gland adeno-

Table 1
Benchmark dose (BMD) values for cancer endpoints in target organs of male mice (2-year cancer bioassay).

Endpoint	Goodness of fit p -value	BMD values (mg/kg bw-day)		References
		BMD _{10%}	BMDL _{10%}	
Harderian gland adenoma, incidence ^a	0.399	0.365	0.173	Beland et al., 2013
Lung adenoma, incidence ^a	0.508	2.10	1.27	
Forestomach squamous cell papilloma, incidence ^a	0.733	4.43	2.92	

^a Log-logistic was the best-fit model.

mas, to 1.27 mg/kg bw-day for the incidence of lung adenomas, and 2.92 mg/kg bw-day for the incidence of forestomach adenomas (Table 1).

4.3. RNA-seq

Analysis of the extent of RNA degradation (i.e., 5'-3' gene-body coverage of RNA-seq reads) using QoRTs (Hartley and Mullikin, 2015) revealed degraded RNA in five samples from the Harderian gland (none for the lung samples). These degraded samples were eliminated from subsequent analyses. Analysis of mdsLog₂ plots across samples from the same dose and time point groups further suggested seven and six outlier samples for the lung and Harderian data sets, respectively. Thus, sample sizes for each group were as follows: 4/group (control and highest dose for day 5 Harderian gland samples); 5/group (12 mg/kg bw-day, day 5, and 3.0 mg/kg bw-day, day 15 Harderian gland samples; and control, 3.0 mg/kg bw-day dose (day 5), and 6.0 mg/kg bw-day dose (day 15) lung samples); and 6/group (rest of the experimental groups).

4.4. Global gene expression changes in the lungs and the harderian glands in response to AA

The number of DEGs for each of the five doses for the three time points in the two tissues is shown in Fig. 2. All DEGs for both tissues are in Supplementary Table S1. The following observations can be made:

- AA exposure caused almost twice as many DEGs in the Harderian glands than in the lungs;
- The maximum number of DEGs in the lungs was 224 (the 24 mg/kg bw-day dose, day 15);
- The maximum number of DEGs in Harderian glands was 427 (the 12 mg/kg bw-day dose, day 31);
- In the lungs, the number of DEGs only showed a dose-dependent increase on day 15;
- In the Harderian glands, the number of AA-induced DEGs exhibited a nonmonotonic or U-shaped dose-response, most notably on day 31 (seen as approximately 3-fold reduction in the number of DEGs at the 1.5- and 12-mg/kg doses), with a nadir at 3 or 6 mg/kg bw-day.

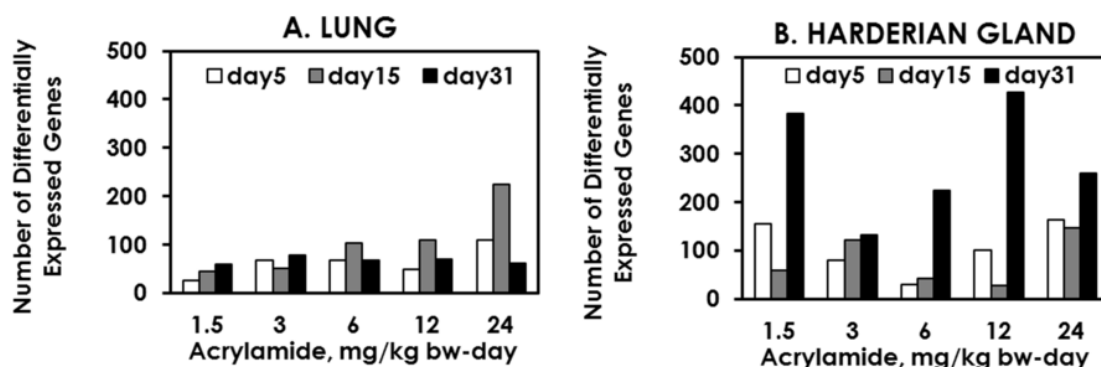


Fig. 2. Number of differentially expressed genes in the lungs and Harderian glands of male CD-1 mice following acrylamide exposure. Genes with p-values < 0.001 and fold-changes > |1.5| were included here.

4.5. Canonical pathways, upstream regulators, and biological functions affected by AA

The results of the IPA “Core Analyses” are summarized in Tables 2–7 and provide information about potential cellular signaling pathways (canonical pathways), upstream regulators, biological functions, and diseases affected by AA in the two mouse target tissues.

Major findings in the lungs include:

- The greatest number of enriched IPA pathways occurred for the highest AA dose group on day 15 (Table 2), in agreement with the greatest number of DEGs on this day (Fig. 2);
- Integrin-linked kinase (ILK) signaling was the most frequently affected pathway in AA-exposed mice, being enriched on both days 5 and 15 (Table 2);
- Inhibited Myocyte Enhancer Factor 2C (Mef2C) and activated lipopolysaccharide (LPS) were the two most prominent upstream regulators (Table 3);
- AA exposure affected diseases and biological functions related to muscle physiology (decreased function and contractility, increased necrosis) and tumorigenicity (increased inflammatory response, aggregation of cells, hypertrophy, organ degeneration and organismal death) (Supplementary Table S3)

Major findings for the Harderian gland include:

- Actin cytoskeleton (AC) signaling and ILK signaling were the most frequently affected (predicted to be activated by the highest dose on day five and downregulated at certain doses on days 15 and 31) pathways following AA exposure, and were perturbed at all three time points (Table 4);
- Tumor necrosis factor (Tnf) was the most frequent upstream regulator of DEGs in the AA-exposed Harderian glands (Table 5; however, note that there were only four upstream regulators predicted to be affected by AA overall);
- Tnf was predicted to be inhibited on day 5, but activated on day 31 (Table 5);
- In agreement with early Tnf inhibition and later activation, “differentiation of cells” was predicted to be inhibited on day 5, but activated on day 31 (Supplementary Table S3);
- Only two IPA “diseases and biological functions” categories were enriched in the mouse Harderian gland following AA exposure (“proliferation of cells” on days 5 and 31 at 3.0 and 6.0 mg/kg bw-day, respectively, and “differentiation of cells” on day 5 at 3.0 mg/kg bw-day (Table 7).

Table 2

Top ten IPA canonical pathways with Fisher’s exact p < 0.05 and Z-score values > |2| for each dose and time point in the lungs of male CD-1 mice exposed to acrylamide in drinking water.

Time point	Acrylamide, mg/kg bw-day				
	1.5	3.0	6.0	12	24
Day 5	None	ILK Signaling (-)	LXR/RXR Activation (-) TREM1 Signaling (+)	None	None
Day 15				ILK Signaling (-) Actin Cytoskeleton Signaling (-) Signaling by Rho Family GTPases (-)	Several Signaling Pathways: Actin Cytoskeleton (-), ILK (-), Integrin (-), RhoA (-), PAK (-), Paxillin (-), Leukocyte Extravasation (-), RhoGDI (+)
Day 31	None				

^aPathways are sorted from lowest to highest Z-score in each category (inhibited or activated). If there were < 10 pathways, they are all shown. ^bActivation (Z-score above +2) or inhibition (Z-score below -2) are shown with (+) and (-), respectively.

Table 3

Top ten IPA upstream regulators with Fisher's exact $p < 0.05$ and Z-score values $> |2|$ for each dose and time point in the lungs of male CD-1 mice exposed to acrylamide in drinking water^a.

Time point	Acrylamide, mg/kg bw-day				
	1.5	3.0	6.0	12	24
Day 5	None	Mef2C (-) ^b Gata4 (-) miR-637 ^c (+)	PD98059 (-) Pparg (-) Dexamethasone (-) Troglitazone (-) Thra (-) Tnfsf12 (+) poly rI:rC-RNA (+) <i>E. coli</i> lipopolysaccharide [LPS, (+)] <i>Salmonella minnesota</i> R595 LPSs (+) Tnf (+)	LPS (+) miR-149-3p (+) miR-4723-5p(+)	Ctnnb1 (-) Agt (-) Forskolin (-) Hipk2 (-) Cisplatin (-) PD98059 (+) miR-331-3p (+) miR-16-5p (+) miR-4755-3p (+) miR-330-5p (+)
Day 15	miR-661 (+)	Egf (-) Cebpa (-) miR-296-5p (+) miR-149-5p (+)	Rosiglitazone (-) Mef2C (-) Stat5B (-) miR-4747-5p (+) miR-661 (+) miR-1275 (+) miR-149-5p (+) miR-6967-5p (+) miR-4525 (+) miR-542-3p (+) let-7a-5p (-) miR-101-3p (-)	Rb1 (-) Srf (-) Mef2C (-) Stat5B (-) Tbx5 (-) Kdm5A (+) miR-361-3p (+) miR-1285-3p (+) miR-1275 (+) miR-1909-3p (+) Egf (-)	Mef2C (-) Myocd (-) Gata4 (-) Rb1 (-) Srf (-) LPS (+) Kdm5A (+) Irfng (+) Pdgf BB (+) miR-328-3p (+) miR-543-3p
Day 31	None	miR-124-3p (-) miR-24-3p (-) miR-320b (-) miR-203a-3p (-) miR-4472 (-) Pkc(s) (+) Decitabine (+)			

^a Regulators are sorted from lowest to highest Z-score in each category (inhibited or activated). If there were < 10 upstream regulators, they are all shown.

^b Activation (Z-score above +2) or inhibition (Z-score below -2) are shown with (+) and (-), respectively.

^c miRNAs with similar seeds are also predicted to be upstream regulators affected by acrylamide.

4.6. Effects observed in lungs

In total, 759 DEGs ("union genes") were affected by at least one dose of AA in mouse lungs (Supplementary Table S1). Nearly half (up to 287 genes on day 15) of these DEGs were related to cancer, which was the top disease/biological function identified by IPA across all time points. The top (based on the number of DEGs) diseases and functional annotations for the lung data were "melanoma" (103 DEGs), "cancer" (287 DEGs), and "melanoma" (94 DEGs) on day 5, 15, and 31, respectively (Supplementary Table S4).

Next, we selected the doses and time points with the greatest transcriptional response (i.e., day 15, top dose for the lung and day 31, 12-mg/kg for the Harderian) in order to find out whether AA perturbs any similar pathways in the two tissues. We found that CS was the top pathway affected by AA when pathways were sorted by the most significant p-value using RNA-seq data from the three target and one non-target tissues of AA-induced carcinogenicity in rodents (Fig. 3). Indeed, many genes that are part of the CS pathway were affected (mostly down-regulated) by AA exposure in the mouse lung, such as troponin T3 and fast skeletal type (*Tnnt3*) (Supplementary Table S5). The most DEGs in the CS pathway in lung (14) occurred on day 15 (there was one and zero affected on days 5 and 31, respectively: Supplementary Table S5). For the affected CS genes, a dose-response was evident based on changes in the two top doses (e.g., *Myh6* and *Ryr2*; Supplementary Table S5). Intriguingly, the ILK and AC Signaling pathways were inhibited by 12mg/kg AA exposure, but activated by 24mg/kg AA on day 5 (Table 4).

4.7. Effects observed in Harderian glands

A total of 1361 DEGs were identified in Harderian gland following AA exposure (Supplementary Table S1). Similar to the lung data, many genes were related to cellular growth and proliferation (Supplementary Table S6). Thus, the most enriched diseases and functions categories were: "proliferation of cells" (34 DEGs), "transport of molecule" (24 DEGs), and "organization of cytoskeleton" (35 DEGs) on day 5, 15, and 31, respectively (Supplementary Table S6).

The effects of AA on the expression of the genes involved in the CS pathway were more prominent in Harderian glands than in the lungs, with more genes affected in the Harderian glands and to a greater extent, compared to lungs (Supplementary Table S5 vs. S7). One peculiar feature in the Harderian glands was the transition from downregulation (1.5–12-mg/kg doses) to upregulation at the top dose for all CS genes affected by AA on day 5 (Supplementary Table S7). This was not observed at the other time points and is conceptually similar to the aforementioned transition from inhibition to activation of the ILK and AC signaling pathways in the lungs.

Comparison of RNA-seq data for AA cancer target (rat thyroid, mouse lung and mouse Harderian) and non-target (rat liver) tissues in rodents.

The data from our study on mouse lungs and Harderian glands were compared to our previous RNA-seq data derived from rat livers and thyroids in male F344 rats following AA exposure in drinking water. The data are available through the Sequence Read Archive (SRA) at <http://www.ncbi.nlm.nih.gov/sra> (bioproject number PRJNA326428). We found that CS and/or its related pathways (AC Signaling and ILK Signaling) were the top cellular signaling pathways affected (mostly, downregulated) by AA in all of the rodent AA cancer target tissues (mouse lungs and Harderian glands, and thyroid glands of F344 male

Table 4
Top ten IPA canonical pathways with Fisher's exact $p < 0.05$ and Z-scores $> |2|$ at each dose and time point in the Harderian glands of male CD-1 mice exposed to acrylamide in drinking water^a.

Time point	Acrylamide, mg/kg bw-day				
	1.5	3.0	6.0	12	24
Day 5	None	None	None	Actin Cytoskeleton (AC) Signaling (-)	Several Signaling Pathways: AC (+), ILK (+), Integrin (+), RhoA (+), Paxillin (+), Rho (+), Signaling by Rho Family GTPases (+) Regulation of Actin-based Motility by Rho (+)
Day 15	AC Signaling (-)	AC Signaling (-)	Nitric Oxide Signaling in the Cardiovascular System (+)	ILK Signaling (-) AC Signaling (-)	Several Signaling Pathways: AC (-), ILK (-), Integrin (-), RhoA (-), Paxillin (-), Rho (-), Leukocyte Extravasation (-) Signaling by Rho Family GTPases (-), RhoGDI (+) Regulation of Actin-based Motility by Rho (-)
Day 31	Several Signaling Pathways: AC (-), ILK (-), RhoA (-), Cardiac Hypertrophy (-), Wnt/ β -catenin (-), iCOS-iCOSL Signaling in T Helper Cells (-), Thrombin (-), PKC θ Signaling in T Lymphocytes (-), Notch (+)			PTEN Signaling (-) AMPK Signaling (-) Notch Signaling (+)	Several Signaling Pathways: AC (-), ILK (-), Integrin (-), CS (-), Chemokine (-), Insulin Receptor (-), AMPK (-), PKC θ Signaling in T Lymphocytes (-), Notch (+), Melatonin Signaling (+) None

^aPathways are sorted from lowest to highest Z-score in each category (inhibited or activated). If there were < 10 pathways, they are all shown. ^bActivation (Z-score above +2) or inhibition (Z-score below -2) are shown with (+) and (-), respectively.

Table 5
Top IPA upstream regulators with Fisher's exact test p-value < 0.05 and Z-scores $> |2|$ at each dose and time point in the Harderian glands of male CD-1 mice exposed to acrylamide in drinking water^a.

Time point	Acrylamide, mg/kg bw-day				
	1.5	3.0	6.0	12	24
Day 5	Tsc2 (+)	None	None	Vcan (-)	Tnf (-)
Day 15	None	None	None	None	None
Day 31	None	None	Tnf (+)	None	None

^aRegulators are sorted from lowest to highest Fisher's exact test p-value. If there were < 10 upstream regulators, they are all shown. ^bActivation (Z-score above +2) or inhibition (Z-score below -2) are shown with (+) and (-), respectively.

rats), but not in the non-target tissue, rat liver (Fig. 3). In all three cancer-target tissues, CS was predicted to be inhibited (negative Z-score, below minus 2) at the doses and time points eliciting the greatest transcriptional response based on the expression of the genes comprising the CS pathway. There were 59 DEGs that were in common between the two tissues in this study that were also altered in the transcriptional profiles of the thyroid glands of male rats dosed with AA in drinking water (Supplementary Table S8). Of the 59 genes, 52 were assigned to "cancer" by IPA, including five genes that belong to the CS pathway: filamin C (*FlnC*), myosin light chain 1 (*Myl1*), phosphorylase kinase gamma subunit 1 (*Phkg1*), protein phosphatase 1 regulatory subunit 3A (*Ppp1r3A*), and ryanodine receptor 1 (*Ryr1*) (Supplementary Table S8).

4.8. RT-PCR validation of select genes in the lungs and harderian glands

Nine genes were selected for RT-PCR validation in the lungs based on their: i) involvement in the CS pathway and/or being detected as differentially expressed by RNA-seq; ii) involvement in AA metabolism to its reactive metabolite GA; and iii) established association with lung cancer. Respectively, these were: i) Actin, alpha 2 (*Acta2*), ATPase, Ca²⁺ transporting, cardiac muscle, fast twitch 1 (*Atp2a1*), Myosin, light polypeptide 1 (*Myl3*), Ryanodine receptor 1 (*Ryr2*), and Troponin T3 (*Tnnt3*); ii) *Cyp2e1*; and iii) Adiponectin (*Adipoq*), Bactericidal/permeability-increasing protein fold containing family A member 1 (*Bpifa1*), and *Bpifb1*. There was good concordance between the two technologies (Supplementary Table S9, Fig. 4) in their ability to detect genes as not being significantly different from the controls (i.e., in 159 out of 180 (88%) cases examined). However, differential expression of four out of the nine genes detected by RNA-seq was not confirmed by RT-PCR (Fig. 4, Supplementary Figs. S1 and S2), making the overall concordance fair overall. Both technologies similarly detected animal-to-animal variability in the data for the majority (six out of nine; gene lists are in Fig. 4) genes examined, evident as good correlation (i.e., R² values for linear trendlines above 0.8) between the individual data points generated by each technology for each animal (data not shown). Importantly, both RT-PCR and RNA-seq detected approximately 2–3-fold decreases in *Cyp2e1* expression.

Six genes were selected for RT-PCR in Harderian glands based on their involvement in the CS pathway and/or being detected as differentially expressed by RNA-seq, or in AA metabolism to GA. These were: Actin, alpha 2 (*Acta2*), ATPase, Ca²⁺ transporting, cardiac muscle, fast

Table 6

Comparison of points of departure (PODs) derived from BMD modeling of apical and toxicogenomics data from male CD-1 mice following acrylamide exposure in drinking water.

Type of data	Endpoint	Origin, time of exposure	POD (mg/kg bw-day)	Corresponding BMD metrics	Reference
Apical	Incidence of Harderian gland adenomas	Harderian gland, 2 years	0.17^{a,b}	BMDL ₁₀	Beland et al., 2013
Toxicogenomics	Incidence of lung adenomas	Lung, 2 years	1.27	BMDL ₁₀	This study
	IPA ^c pathway "Oxidative Phosphorylation"	Harderian, 31 days	0.54^{b,d}	BMDL median	
	IPA pathway "Death Receptor Signaling"	Lung, 15 days	2.21 ^d	BMDL median	

^a The lowest POD value from male mice, reported in Table 1 above.

^b The most relevant and lowest values for both types of data are in **bold**.

^c IPA cellular signaling pathway.

^d The lowest BMDL median values for the IPA pathway for each tissue (reported in Supplementary Tables S11 and S12).

Table 7

Summary of toxicogenomics data derived from this study for the genotoxic and calcium signaling [CSJ] modes of actions (MOAs) for acrylamide (AA) carcinogenicity in mouse lungs and Harderian glands.

MOA	Supporting data	Inconsistent data	Missing data
GENOTOXIC	<ul style="list-style-type: none"> ● Decreased expression of <i>Cyp2e1</i> in the lungs on both days 15 and 31 	<ul style="list-style-type: none"> ● Effect on <i>Cyp2e1</i> was seen in the lung only, suggesting that the MOA may be irrelevant for the carcinogenic MOA operating in the Harderian glands ● <i>Cyp2e1</i> expression in the lung was downregulated, rather than upregulated, as in the case of the rat thyroid (Chepelev et al., 2017), complicating understanding of the role of <i>Cyp2e1</i> in AA carcinogenicity in the mouse lung ● Detection of DNA adducts in the lung, liver, and kidney of female rats (Watzek et al., 2012) despite the lack of tumors in these organs in cancer bioassays 	<ul style="list-style-type: none"> ● <i>Cyp2e1</i> enzyme assays may be more informative and direct indications of the extent of AA metabolism by <i>Cyp2e1</i> than relative <i>Cyp2e1</i> transcript levels ● Genotoxicity testing data from the target tissue (e.g., Harderian gland DNA adducts)

Table 7 (Continued)

MOA	Supporting data	Inconsistent data	Missing data
	<ul style="list-style-type: none"> ● <i>Cyp2e1</i> BMDL on day 15 was 1.17 mg/kg bw-day, in good dose-response concordance with cancer (e.g., AA metabolism by <i>Cyp2e1</i> to genotoxic metabolite GA) 	<ul style="list-style-type: none"> ● No effect of AA on the genes and pathways related to DNA-damage response that are typically induced by genotoxic carcinogens. For example, in the case of the genotoxic carcinogen benzo[a]pyrene, affected IPA pathways (that had at least five genes per a pathway that could be modeled) following both three- and 28-day repeated daily oral exposures were: p53 signaling, Cell cycle: G1/S checkpoint regulation, Cell cycle: G2/M checkpoint regulation, and Cell cycle control of chromosomal replication (Moffat et al., 2015). None of these were affected by AA in either tissue (see Supplementary Tables S9 and S10, for example) 	<ul style="list-style-type: none"> ● Cancer bioassays and sub-chronic studies on the Harderian gland to determine if there is increased incidence of adenomas at doses lower than those used here and in the previous cancer bioassay (Beland et al., 2013) and covering the range of typical human exposure (i.e., starting at least as low as 0.5–3.4 µg/kg (EFSA Panel on Contaminants in the Food Chain (CONTAM), 2015). These studies are necessary to establish appropriate dose-response concordance between proposed KEs and adverse outcome (cancer), as well as to consider background level of DNA lesions in humans for human health risk assessment, as suggested elsewhere (Watzek et al., 2012)

Table 7 (Continued)

MOA	Supporting data	Inconsistent data	Missing data
CS-BASED	<ul style="list-style-type: none"> ● CS and the pathways with which CS shares many genes (Actin Cytoskeleton Signaling and ILK Signaling) were the top affected pathways in this study, in both tissues, and in the previous study in rat target (thyroid), but not non-target (liver) tissues (Fig. 4) ● Altered CS is in agreement with skeletal muscle being a target of AA toxicity (Maronpot et al., 2015) and in agreement with many reports of reduced calcium content in the malignant tumor tissues (see Discussion for references) 	<ul style="list-style-type: none"> ● CS was not the most sensitive (i.e., with the lowest BMDL median values) pathway in the lung (albeit, one of the top, See Supplementary Table S9) and in the Harderian glands (Supplementary Table S10) ● The concordance between the BMD values for the CS pathway with the cancer BMD is not as strong for the Harderian gland (2.62 vs. 0.17 mg/kg bw-day, Table 1 and S10) than that for the lung (3.09 vs. 1.27 mg/kg bw-day, Tables 1 and 8) 	<ul style="list-style-type: none"> ● Data to enrich our mechanistic understanding of the factor(s) affecting reduced expression of CS genes; this (these) could be molecular initiating event(s) in the carcinogenic MOA(s) of AA ● Biochemistry data on the levels of intracellular Ca²⁺ and CS proteins, and cytoskeleton integrity data in the mouse lung and Harderian glands following AA exposure

Table 7 (Continued)

MOA	Supporting data	Inconsistent data	Missing data
	<ul style="list-style-type: none"> In agreement with previously reported effects of AA on structural proteins (microtubules and microfilaments) and on CS in many neurotoxicity studies (reviewed in Introduction). 		<ul style="list-style-type: none"> Data supporting temporal concordance of the proposed MOA (i.e., are KEs observed in the expected order?). Data presented herein are primarily measuring changes in KE1 and KE2, which can be described by transcriptional changes. We show by upstream regulatory analysis that KE1 (Mef2c) is likely inhibited, which is concurrent with KE2, alterations in CS transcripts (Fig. 1). These are clearly occurring before the adverse outcome, cancer (other studies). However, temporal analysis of the other KEs is not possible from the present or existing data and is a significant gap. Missing data that should be collected include levels of Mef2c and its oxidized form, protein levels for the CS genes, calcium levels, and other biochemical changes that can measure the respective KEs to assess temporal relationships.

twitch 1 (*Atp2a1*), Myosin, light polypeptide 1 (*Myl1*), Ryanodine receptor 1 (*Ryr1*), Troponin T3 (*Tnnt3*), and *Cyp2e1*. Again, there was good concordance between the two technologies both in their ability to measure non-changing genes (i.e., in 115 out of 180 (64%) (Fig. 4) cases examined). More importantly of the six genes examined, five (i.e., all but *Acta2*, which was not differentially expressed as measured by RNA-Seq either) were confirmed as differentially expressed by RT-PCR. Based on RNA-Seq of *Cyp2e1*, even its 'basal' levels were below the 0.5

count per million cut-off, precluding statistical analyses of these data. RT-PCR revealed decreased *Cyp2e1* expression that ranged from 16- to 1.7-fold on day 31 (Supplementary Table S10) compared to the control. The expression of *Cyp2e1* showed a U-shaped dose-response curve as was noted above for all three time points for the number of DEGs across AA doses (Fig. 2). Also, the magnitude of *Cyp2e1* downregulation in the Harderian gland was up to five times greater than that observed in the lungs (i.e., up to 3.8-fold decrease) by both technologies (Supplementary Table S9 vs. S10).

4.9. BMD analysis of RNA-seq data

The IPA canonical pathways with their corresponding BMDL median values in the lungs and Harderian glands are shown in Supplementary Tables S11 and S12, respectively. BMDL median values were computed for cellular signaling pathways with at least five genes per pathway that could be modeled, which is a standard threshold that has been used in studies aimed at informing health risk assessment (Thomas et al., 2011). Here, an ANOVA filter ($p < 0.05$ for treated versus control samples) was applied prior to the BMD modeling of individual genes, and a minimum of five genes that could be modeled in BMDEpress, was a prerequisite for considering a pathway as being significantly affected by AA (another criterion was a Fisher's Exact Test $p < 0.1$). Therefore, each pathway shown in Supplementary Tables S11 and S12 has at least five genes exhibiting a dose-related effect, which is helpful for understanding transcriptomic dose-response in the two mouse tissues due to AA exposure. All of the pathways reported in Supplementary Tables S11 and S12 had BMD/BMDL ratios < 3 , indicating good model fits. The pathways with the lowest BMDL median values were computed for the time points that showed the greatest transcriptional response (i.e., greatest number of DEGs; this was day 15 for the lungs and day 31 for the Harderian glands). The pathway with the lowest BMDLs in the lungs was Death Receptor Signaling (BMDL median of 2.21 mg/kg bw-day) (Supplementary Table S11), and in Harderian glands was Oxidative Phosphorylation (BMDL median of 0.54 mg/kg bw-day) (Supplementary Table S12). The BMDL median of the CS pathway in the lungs was 3.09 mg/kg bw-day (Supplementary Table S11). The BMDL median of the CS pathway in the Harderian glands on day 31 was 2.62 mg/kg bw-day; the pathway had eight genes that were modeled in BMDEpress, out of the 179 genes comprising the CS pathway in IPA, but the Fisher's exact test p-value was 0.41; hence, the pathway BMDL values were not reported in Supplementary Table S12.

5. Discussion

We conducted functional annotation analyses and BMD modeling of RNA-seq data to gain better mechanistic understanding of the carcinogenic MOA of AA in the lungs and Harderian glands of male mice. This analysis revealed enrichment of the CS pathway among the DEGs following AA exposure in these tissues, which was consistent with AA-induced effects in thyroid tissue in rats. A detailed MOA analysis revealed limited support for genotoxicity as a KE in the AA-induced cancer MOA for these tissues, but supported a role for CS in both tissues. This finding is in agreement with observations on AA-induced neuropathies decades earlier and our recent work showing that the CS-based MOA is biologically plausible for AA-induced thyroid cancer in male rats, based on a weight-of-evidence analysis. This accumulating evidence, together with well-documented reductions in calcium in malignant tumors in rodents and humans, suggests that perturbed expression of CS is a KE in the cancer MOA mediated by AA in rodent tissues.

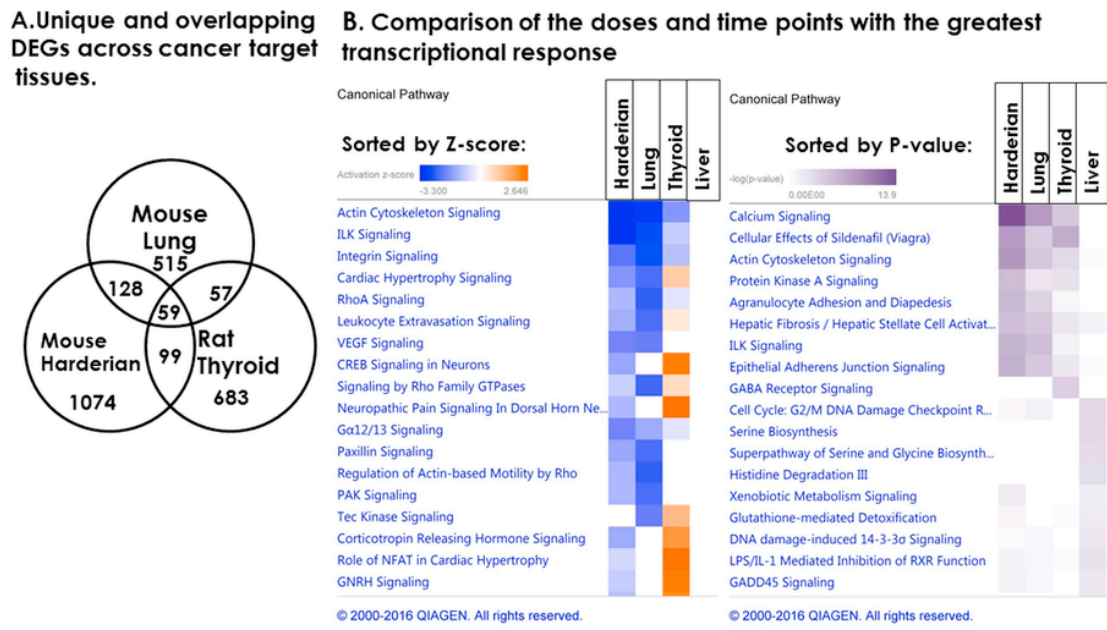
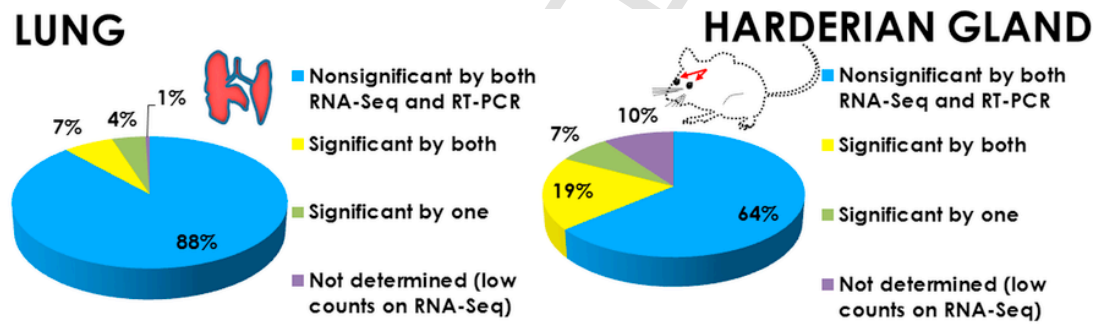


Fig. 3. Comparison of the RNA-seq data sets for the AA target and non-target tissues in the male CD-1 mice and male F344 rats. A. Venn diagram, showing overlapping and distinct differentially expressed (p-values < 0.001 and fold-changes > |1.5|) genes in the three target tissues. B. Results of the “Comparison Analysis” performed using IPA software on the differentially expressed genes (p-values < 0.001 and fold-changes > |1.5|) for the target (mouse Harderian gland, mouse lung, and rat thyroid) and non-target (rat liver) tissues. Complete datasets for the RNA-seq of rat tissues are available at the Sequence Read Archive (SRA) at <http://www.ncbi.nlm.nih.gov/sra>, bioproject number PRJNA326428. The doses and time points with the greatest transcriptional responses (i.e., number of differentially expressed genes, Fig. 2) were selected for the comparison and were: day 31, 12mg/kg bw-day (mouse Harderian); day 15, 24mg/kg bw-day (mouse lung); day 15, 6.0mg/kg bw-day (rat thyroid); and day 31, 12mg/kg bw-day (rat liver).



Shown in pie charts are percent out of 180 simultaneous comparisons for each tissue*

COMPARISON PARAMETER	LUNG	HARDERIAN
Genes examined by RT-PCR	9** [Acta2, Adipoq, Atp2a1, Bpifa1, Bpifb1, Cyp2e1, Myl3, Ryr2, Tnni3]	6 [Acta2, Atp2a1, Cyp2e1, Myl1, Ryr1, Tnni3]
Genes differentially expressed by RNA-Seq (any dose, time point)	9 [all of the above]	4 [all 6 above, but Acta2 and Cyp2e1]
Genes differentially expressed by RT-PCR (any dose, time point)	4 [Adipoq, Bpifb1, Cyp2e1, Ryr2]	5 [Atp2a1, Cyp2e1, Myl1, Ryr1, Tnni3]
Genes with high correlated ($R^2 > 0.8$ (trendline in excel), between individual animals) for both technologies***	6 [Adipoq, Atp2a1, Bpifa1, Bpifb1, Myl3, Tnni3]	5 [Atp2a1, Cyp2e1, Myl1, Ryr1, Tnni3]

*number of genes x 3 data points x 5 doses x 2 technologies [Supplementary Tables S7 and S8]; ** not all genes were examined at all data points for the lung; see Supplementary Table S7 for details; *** data not shown.

Fig. 4. Comparison of RNA-Seq and RT-PCR data. Data for the genes examined by both RNA-seq and RT-PCR were compared in terms of the number of times each technology detected the expression of the gene as being non- or significantly different from the time-matched controls, out of the 180 simultaneous comparisons (pie charts), as well as the overall concordance between the two technologies (table of the comparison parameters).

5.1. Application of Bradford-Hill criteria to compare genotoxicity vs CS-based MOAs

We used our data to examine several modified Bradford-Hill considerations to determine the level of support for both MOAs (Meek et al., 2014): biological plausibility and empirical evidence of temporal- and dose-response concordance (Table 7). The latter refers to observation

of the hypothesized KEs at doses occurring below or similar to those associated with an adverse outcome (Meek et al., 2014) and is discussed as a part of “Empirical evidence” in the BMD comparison of relevant endpoints for both MOAs. This is a part of the MOA/human relevance (MOA/HR) framework that is applicable to both traditional and toxicogenomics data [e.g. (Moffat et al., 2015)]. In addition to our own data, previous reviews ((Dourson et al., 2008, US Environmental Protection Agency (EPA), 2010, EFSA Panel on Contaminants in the

Food Chain (CONTAM), 2015) on AA were used for summarizing and interpreting traditional AA toxicity data, as well as the only other toxicogenomics study on AA in rats that we could identify (Bowyer et al., 2008).

Table 7 highlights several inconsistencies we identified while assessing the empirical data for the genotoxicity MOA. These include the presence of GA DNA adducts in cancer non-target tissues of female rats (Watzek et al., 2012), the lack of an effect of AA on the expression of *Cyp2e1* in the Harderian gland (required for genotoxicity), and the lack of effect on the expression of the many classical DNA-damage inducible genes in both tissues. However, it should be noted that *Cyp2e1* induction by its substrates is complicated by the fact that *Cyp2e1* is regulated by transcriptional, post-transcriptional, translational, and post-translational mechanisms (Novak and Woodcroft, 2000). On the other hand, CS genes were consistently altered in cancer target tissues following AA exposure, but not in the non-target tissue.

5.2. Genotoxicity as a KE in the MOA of AA-induced cancer

5.2.1. Biological plausibility

It is well established that genotoxicity can lead to tumorigenicity. In addition, it is broadly accepted that AA exposure can cause GA-DNA adducts and genotoxicity. Thus, it is biologically plausible that AA causes cancer through a genotoxic MOA. However, AA-DNA adducts have never been observed [reviewed in (EFSA Panel on Contaminants in the Food Chain (CONTAM), 2015)], and it is clear that AA needs to be metabolized by *Cyp2e1* to be able to lead to GA-DNA adduct formation. Broadly speaking, it is thus biologically plausible that AA causes cancer through a genotoxic MOA. However, there are inconsistent findings of AA-induced genotoxicity in rodents. For example, the lack of genotoxicity at doses that cause cancer in 2-year cancer bioassays suggests that non-genotoxic mechanisms contribute to acrylamide-induced carcinogenicity in rodents (Dobrovolsky V.N. et al., 2016, Hobbs et al., 2016). Overall, although genotoxicity is a well-established path to cancer, the aforementioned inconsistencies add some degree of uncertainty to the biological plausibility of the genotoxicity-based MOA of AA.

5.2.2. Empirical evidence

A variety of inconsistencies associated with the ability of AA to induce genotoxicity and cause of cancer (Fig. 1) have been introduced above. Very generally, despite the conclusion that AA is “clearly genotoxic in somatic and germ cells” *in vivo* [reviewed in (EFSA Panel on Contaminants in the Food Chain (CONTAM), 2015)], the empirical evidence shows that AA-induced genotoxicity is apparent only at high doses (Mei et al., 2008, Dobrovolsky V.N. et al., 2016, Hobbs et al., 2016), well above doses that cause cancer. For example, a two-month drinking water study in male Big Blue rats revealed a weak positive effect on mutant frequency in the *cII* mutant assay in the thyroid only at the high (approximately 10 mg/kg bw-day), but not medium (approximately 5.0 mg/kg bw-day) dose. Similarly, there was no effect on *cII*

mutant frequency in either testis, or mammary gland (Mei et al., 2010), both of which are targets of AA carcinogenicity. Thus, genotoxicity may be an associated biological event that is not necessarily key to the MOA of AA-induced carcinogenicity.

To explore dose-concordance in more detail using our own data, we compared BMDL values for the lung and Harderian adenomas (Table 1) to those from our toxicogenomic data. For this, we compared BMD modeling values for the cancer endpoints to those of genes within the p53 Signaling pathway (Table 8), which was chosen based on its well-established biological relevance to the genotoxic MOA. We first noted that the p53 Signaling pathway did not pass standard filtering thresholds used in transcriptional BMD modeling (i.e., requiring at least 5 genes per pathway that could be modeled and Fisher's exact test p-values < 0.05). In addition, we compared the transcriptomic data for AA to published gene expression profiles for two classical aeneugens, colcemid and vincristine, using Illumina's Correlation Engine knowledgebase. A transcriptomic study in TK6 cells (Kuehner et al., 2013) was identified for this purpose as there was no *in vivo* rodent study. As expected, the two aeneugens altered the expression of DNA repair, cell cycle, and mitosis-related genes (Supplementary Fig. S3). However, the pathways induced were not consistent with the effects caused by AA exposure in mice and rats. These findings, combined with the lack of shared genotoxic pathways affected by AA across the three target tissues (Fig. 3), do not support genotoxicity as a central KE in the MOA for AA-induced cancer.

5.2.3. Data gaps

Further support for this conclusion could be provided through investigations of DNA adducts, MN, and DNA strand break measurements in rodent target tissues.

5.3. CS as KE in the MOA of AA-induced carcinogenicity

5.3.1. Biological plausibility

Experiments to investigate the role of calcium in carcinogenesis can be traced back to the 1900s. For example, ash analysis of human malignant tumors, obtained from operations or *post mortem*, showed that malignant tumors contained less calcium than similar normal tissues (Beebe, 1904). Similar results were obtained by an analysis of “Jensen tumor mice”, in which rapidly growing tumors contained low or undetectable amounts of calcium, while slowly growing tumors had elevated calcium content (Clowes and Frisbie, 1905). For chemically induced tumors, a single application of the carcinogen methylcholanthrene reduced the concentration of calcium in mouse epidermis to 50% within 10 days, and reduced calcium content in mouse carcinomas to approximately 25% of normal, non-malignant epidermis (Carruthers and Suntzeff, 1944). This revealed two distinct phases: an immediate reduction in calcium content of the mouse epidermis, which lasted for many weeks, and a further reduction in calcium content

Table 8

Comparison of the BMD values for the genotoxic^a and calcium signaling [CS] modes of actions (MOAs) for acrylamide (AA) carcinogenicity in mouse lungs and Harderian glands.

Organ	IPA Pathway	Fishers Exact Test p-value	Number of significant genes modeled	BMDL _{1SD} Median (mg/kg bw-day)	BMD _{1SD} Median
Harderian gland	p53 signaling	0.556	4 ^b	4.42	10.8
	Calcium Signaling	0.406	8	2.62	3.98
Lung	p53 signaling	0.733	1 ^b	N.A. ^c	
	Calcium Signaling	0.04	11	2.81	3.09

^a The p53 pathway (related to the genotoxic MOA) had fewer than the generally accepted of genes (recommended minimum is 5 genes) that could be modeled, and the pathway was not significantly enriched (Fishers Exact p-value < 0.05). The statistical threshold for including genes for BMD modeling was an ANOVA p < 0.05 (unadjusted) for at least one dose relative to controls.

^b Genes that belonged to this pathway were: *Ep300*, *Gadd45a*, *Pik3r1*, and *Pik3c2b* (Harderian) and *Pik3c2a* (lung).

^c N.A., not available; only one gene (*Pik3c2b*) could be modeled here (BMDL is 3.91 and BMD 7.92 mg/kg bw-day), hence median values for the pathway cannot be calculated.

when the epithelial cells were transformed into cancer cells (Carruthers and Suntzeff, 1944). By the 1970s, it was recognized that reduced calcium content of cancer cells was correlated with their reduced adhesiveness, increased mobility, and increased permeability; therefore, calcium was viewed as a key to greater understanding of the process of carcinogenesis (Miller, 1977).

Currently, the involvement of CS in major cell signaling pathways related to various types of cancer is firmly established (Bidaux et al., 2007; Marchi and Pinton, 2016; Monteith et al., 2017). Furthermore, a current review of the role of calcium in carcinogenesis led to the hypothesis that mutations in a “pool” of CS genes may be considered as a “driver” for cancer progression (Hoth, 2016). One important CS gene within this “pool” is *Atp2a1* (SERCA1 in humans), an intracellular calcium pump that brings Ca^{2+} from the cytosol to the endoplasmic reticulum (ER). This gene was downregulated in response to AA in the three target tissues in our study (Supplementary Table S1). One functional consequence of this downregulation could be perturbation of the calcium gradient. This can lead to anti-oncogenic (increased cytosolic calcium levels, apoptosis (Chemaly et al., 2018)), and pro-oncogenic (increased proliferation, migration, metastasis, and invasion of cancer cells (Hoth, 2016)) consequences. Similarly to *Atp2a1* downregulation observed in our studies, decreased expression of *SERCA3* was found in gastric, lung, and choroid plexus tumors, and in myeloid leukemia [Reviewed in (Dang and Rao, 2016)]. Overall, our findings support the plausibility of altered CS as a KE leading to cancer.

It is well established in the field of neurotoxicology that AA exposure alters CS [e.g. (Reagan et al., 1994)]. However, how exactly disruptions of CS by AA (or other carcinogens) lead to neoplasia is poorly understood, perhaps in part due to the plethora of biochemical processes in which Ca^{2+} participates. Indeed, CS can be mechanistically linked to each hallmark of cancer (Stewart et al., 2015). Furthermore, alterations in Ca^{2+} homeostasis can be related to the key characteristic of carcinogens #10 (alteration in cell proliferation, cell death, or nutrient supply) (Smith et al., 2016). Nonetheless, the plausibility of AA-induced perturbations in CS as a critical KE in the MOA of AA-induced cancer has not been firmly established. This and other studies (Chepelev et al., 2017; Recio et al., 2017) have generated data that are consistent with the premise that CS pathways may be altered by AA exposure in other tissues, and have suggested that this may be important for carcinogenesis, thus paving the way for further studies.

5.3.2. Empirical evidence

As described above, several studies have demonstrated that AA interacts with cytoskeletal proteins (Lapadula et al., 1989; Sickles et al., 1995, 1996, 2002, 2007), many of which are also part of the CS. Inhibition of the CS pathway was also observed in the thyroids of male SD rats as a result of an 8-week iodide deficiency diet, and has been proposed to be an adaptive response that cells deploy to control epithelial growth and proliferation in response to excessive thyroid hormone stimulation (McDougal et al., 2011). However, the toxicological significance of the inhibition of the CS pathway by AA to its carcinogenic MOA requires further studies. Furthermore, inhibition of the CS pathway, reported here in both tissues, is consistent with many reports of reduced calcium content in malignant tumor tissues. Moreover, the empirical evidence that AA exposure alters CS is clearly defined/accepted in the field of neurotoxicology. Perturbation of CS at early (i.e., 5 or 15–30 days) time points in the present study are consistent with an earlier report (Carruthers and Suntzeff, 1944) of an immediate (i.e., evident within 10 days of a single application of methylcholanthrene) cellular response to a chemical carcinogen that is manifested as reduced calcium levels in the mouse epidermis following a carcinogen application. Our time series data demonstrate consistent effects of AA on genes in the CS and related pathways (ILK and AC Signaling) on days 5 (Harderian only), 15 (both tissues), and 31 (Harderian only). These

data at early time points are consistent with the aforementioned early cellular response to a carcinogen exposure (Carruthers and Suntzeff, 1944), i.e., reduction in tissue calcium content. This is consistent with our proposal (Fig. 1) that perturbed CS is an early KE. Other than that, more data are required to scrutinize the temporal concordance (i.e., whether the proposed KEs occur in the expected order) of the proposed MOA, as described in Table 7. Originally, sampling on days 5, 15, and 31 was carried out to provide preliminary data for such temporal concordance analysis for genotoxicity endpoints. However, our toxicogenomic data pointed to this novel CS-mediated MOA, and the transcriptional changes can only be used as an indirect measure of KE1, and a direct measure KE2. We are not able to measure the MIE or KE3 using transcriptional profiling, as indicated in Table 7. Interestingly, the CS and related pathways were activated in response to AA at day 5, but inhibited on days 15 and 31 (Table 4). This suggests that toxicogenomic experiments with time series similar to ours are capable of capturing some dynamic transcriptional responses that may be mechanistically informative for MOA development. Most importantly, the robust effect of AA on the CS and its related pathways, AC and ILK Signaling, across target tissues and two different species in our studies, in parallel with lack of effect in a non-target tissue (rat liver), provides empirical evidence in support of this CS-mediated MOA.

Comparison of cancer (Table 1) and toxicogenomic BMD values for the CS pathway (Table 8) indicates that the former were approximately 11 and 1.5 times higher than the BMD values for cancer endpoints. BMDL medians generally tend to be slightly higher (but within 10-fold) of the BMDLs for apical endpoints (Farmahin et al., 2016) and the present values are within the expected range. However, we believe that comparisons of BMDs should be approached with caution. Slob (2017) recently demonstrated that differences in response maxima across endpoints require the determination and use of endpoint-specific benchmark response values. For example, cancer is a discrete categorical endpoint and the maximum response would be 100%. In contrast, gene expression, a continuous variable, can have highly varying theoretical maximum responses (e.g., from 100% to 10,000%) (Chepelev et al., 2015a,b)]. Moreover, each pathway BMDL represents the overall median of all the genes in a pathway, and thus does not represent the most responsive genes. For example, the CS pathway, as defined by IPA, contains 179 genes and it is possible that only a few of those are directly relevant to the carcinogenic MOA of AA studied here.

The fact that CS is consistently affected by AA in the target tissues and two species lends strong support to the CS-based MOA, even though BMD modeling of the CS does not provide strong support for this MOA. Indeed, CS and the related AC and ILK Signaling pathways were the top affected (mostly, downregulated) pathways in this study in both tissues and in the rat thyroid (Fig. 3). However, CS and its related pathways were unaffected in the non-target tissue, liver, in the male Fischer 344 rats (Fig. 3). As many of the CS genes play a role in skeletal muscle functions, our results are consistent with an earlier report of skeletal muscle being a target of AA toxicity (Maronpot et al., 2015). This finding complements earlier reports of AA interaction with cytoskeletal proteins (Lapadula et al., 1989; Sickles et al., 1995, 1996, 2007).

5.3.3. Data gaps

An important experiment will be to measure physiological changes in CS in response to AA over time in AA-exposed rodent tissues. Supplementation or exacerbation of this pathway to assess its effects on carcinogenesis will also be critical to determining the essentiality of elements of this proposed MOA. Another factor that remains to be elucidated is the molecular initiating event that leads to the observed changes in the expression of CS genes, i.e., how (or whether) these observed transcriptomic changes originate from well-described covalent binding of AA to cytoskeletal proteins as observed in earlier studies.

One potential explanation to the aforementioned question is adduct formation, through Cys oxidation, between AA and a key protein, such as transcription factor Mef2, leading to loss of its function. Mef2 factors regulate the expression of many CS genes, and Mef2c was predicted to be inhibited by AA in the lung (Table 3) and in the rat thyroid (Chepelev et al., 2017). Mef2C is highly conserved across species and Mef2C in human embryonic kidney (HEK) 293 cells undergoes oxidative modification (S-nitrosylation) at Cys39, which leads to compromised Mef2C-DNA binding, reduced transcriptional activity, and increased apoptosis of neurons in conditional Mef2C knock-out in the mouse brain (Okamoto et al., 2014). Therefore, Mef2 transcription factors should be the subject of future studies of AA toxicity as they may provide a link between the neurodegenerative and carcinogenic properties of AA. Another example of a key signaling protein with Cys residues prone to oxidation that also belongs to the CS pathway is Ryr1 (Sun et al., 2013). Overall, whether AA forms adducts with Mef2C or Ryr1 to render them inactive requires further studies. It is worth noting that AA perturbed the expression of <10–20% of the genes associated with the pathways reported in Supplementary Tables S11 and S12. In addition had a single time point been used, much of the transcriptomic results that were shared by the two tissues analyzed here would have been missed (most critically, the proposed CS-based MOA). Thus, appropriate study design to establish MOA across tissues for a chemical is challenging. However, there is accumulating evidence that sampling time is not as important for simply establishing a transcriptomic POD (Farmahin et al., 2016) as opposed to defining a MOA. Our study supports this notion, as described below (all the lowest BMDs across the time points are within 10-fold of each other).

In addition, we highlight the nonmonotonic transcriptomic response to AA exhibited in the Harderian glands (Fig. 2B). This response shares striking similarity to the response of the rat thyroid to AA described by our group earlier (Chepelev et al., 2017) and also observed in the mouse urinary bladder in response to arsenite (Clewell et al., 2011), a carcinogen with threshold effects whose MOA includes arsenite interaction with cellular sulfhydryl groups (Cohen et al., 2013). In addition, as noted above, in the Harderian glands there was a transition from down- (1.5–12-mg doses) to upregulation (top dose) on day 5 for all CS genes affected (Supplementary Table S5). A similar effect, a transition from inhibition to activation of the AC signaling pathway that is related to CS, was also evident in the lungs (12- vs. 24-mg/kg dose on day 5, see Table 4). A similar effect, i.e., change from down- to upregulation, was observed for several genes in the aforementioned arsenite transcriptomic study of Clewell and co-workers. The similarity in the shape of the transcriptomic dose-response curve observed here for AA and elsewhere for arsenite (Clewell et al., 2011) adds evidence in support of the proposed MOA, based on the AA or GA interaction with Cys-rich proteins (Fig. 1). A clear explanation for these trends has yet to be put forth. Overall, the major gap at present is the lack of phenotypic characterization of the effects of AA on CS (e.g., measurements of intracellular Ca^{2+} levels, and assessment of cytoskeleton and integrity, over longer exposure times). This is a limitation of the present work and future studies are required to confirm that the transcriptional perturbations measured in rats and mice on CS genes translate into frank effects.

5.4. POD derivation

Administration of all the doses led to significant increases in tumor incidence in the mouse Harderian gland and all but the lowest dose led to increased lung tumors in the cancer bioassay (Beland et al., 2013). The dose range was selected in our study to ensure that we did not miss the manifestation of a transcriptional response associated with DNA damage, given that our previous study in mice (Hobbs et al., 2016) could not detect genotoxicity by the MN and Pig-a assay at doses

below 6.0 and 3.0 mg/kg bw-day, respectively. Nonetheless, future studies covering the range of human exposure (i.e., 0.5–3.4 μ g/kg (EFSA Panel on Contaminants in the Food Chain (CONTAM), 2015) are required to scrutinize the dose-response concordance between proposed KEs and adverse outcome (cancer), as well as to consider background level of DNA lesions in humans for human health risk assessment.

The pathway with the lowest median BMDL has been proposed as a conservative approach to derive a toxicogenomics POD (Thomas et al., 2011). Using this approach, our toxicogenomic-informed PODs for both tissues would be based on the median BMDL values for the IPA pathways “Death Receptor Signaling” (lung) and “Oxidative Phosphorylation” (Harderian gland). The corresponding median BMDLs of the two pathways are 2.21 and 0.54 mg/kg bw-day, respectively, and are within 3-fold of the BMDLs derived from the 2-year cancer bioassay data, 1.27 and 0.17 mg/kg bw-day, respectively (Table 6). In addition, the toxicogenomic PODs that could be derived from the two tissues are in good agreement with the POD of 0.43 mg/kg bw-day, calculated as the BMDL₁₀ from the data on the incidence of peripheral nerve (sciatic) axonal degeneration in male F344 rats exposed to AA in drinking water daily, for two years (EFSA Panel on Contaminants in the Food Chain (CONTAM), 2015).

To further explore the use of transcriptional perturbations as a POD in regulatory decision-making, we derived BMDs for altered pathways in both rats and mice from all tissues in all of our AA data sets. We examined the relationship between PODs derived from transcriptomics and those derived from apical endpoints (i.e., cancer). It has been proposed that transcriptional PODs are conservative estimates of the dose at which biological perturbations begin occur, and thus would provide a suitable exposure threshold regardless of knowledge of the MOA (Farmahin et al., 2016). Overall, the toxicogenomic data for the most sensitive pathways (i.e., with the lowest BMDLs, provided at least five genes per pathway could be modeled and Fisher's exact test p -value < 0.05) generated in this and our previous studies in rats provide a very close ($R^2 = 0.77$) approximation to the cancer PODs (Fig. 5), illustrating the utility of toxicogenomics in quantitative human health risk assessment, especially for chemicals lacking data from established toxicity tests.

5.5. Potential human relevance

We previously discussed the similarity between downregulation of the CS gene parvalbumin (*PVALB*), one of the two biomarkers of the thyroid (Hürthle cell) adenoma and carcinoma in humans (Cerutti et al., 2011), and in the rat thyroid in response to AA exposure (Chepelev et al., 2017). Similarly, *Pvalb* was strongly downregulated (e.g., over 2000-fold on day 31 at the 12-mg dose) in this study in the mouse Harderian. Due to the lack of this gland in humans, direct transcriptome comparison of mouse profiling from this study to that from human tumor samples is not appropriate. For the lung, such a meta-analysis using the default settings of the Illumina “Correlation Engine” of the dose eliciting the greatest transcriptional response (i.e., the highest dose on day 15) across human studies (query performed with “*Homo sapiens*” and “lung” set as filters), identified gene expression profiles from lung squamous cell carcinoma patients [GSE26051 (Edgar et al., 2002)] as most similar to the AA-treated mouse lungs. There were 156 overlapping genes in the studies, with a positive correlation and highly significant p -values for the Fisher's exact test (data not shown). Out of the overlapping genes, eight are involved in CS (*Actn2*), bestrophin 1 (*Best1*), calsequestrin (*Casq2*), hippocalcin-like 4 (*Hpcal4*), *Ryr2*, sarcalumenin (*Srl*), titin (*Ttn*), and troponin C, cardiac/slow skeletal (*Tnnc1*). These were all downregulated, as were the majority of the differentially expressed CS genes identified in this and previous (Chepelev

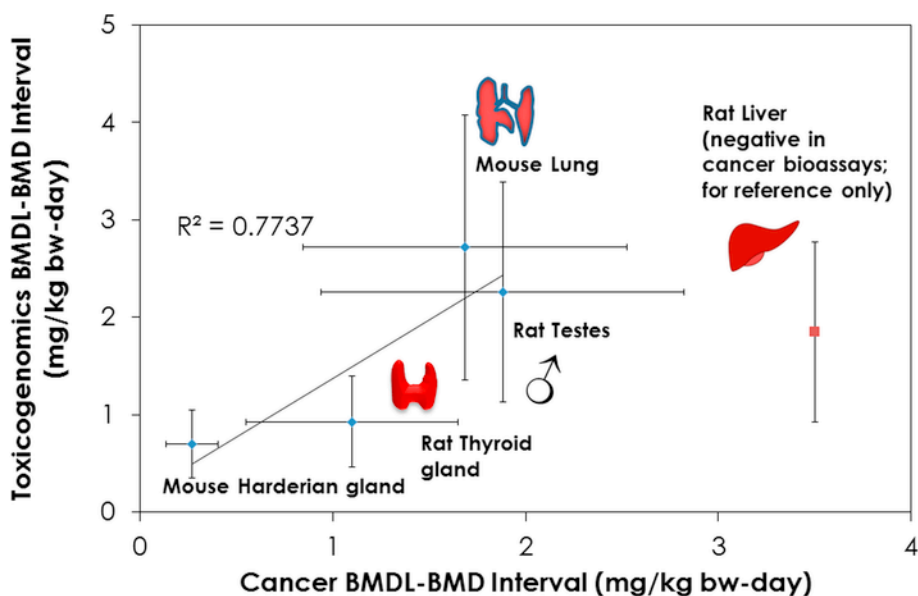


Fig. 5. Comparison of cancer and toxicogenomic BMD modeling data. The BMDL-BMD intervals for each organ for both cancer and toxicogenomic data are shown to show the confidence on the BMD estimation. Cancer data are from (Beland et al., 2013) (the lowest BMD data from all four cancer bioassays). Toxicogenomic data from mouse lungs and Harderian glands are from this study; rat thyroid and liver are from (Recio et al., 2017; Chepelev et al., 2017). Toxicogenomic data from the rat liver are shown, but there is no corresponding cancer endpoint, as liver was negative in all four cancer bioassays at the doses tested (≤ 3.0 mg/kg bw-day); therefore, rat data are shown here for reference only. The purpose of this analysis is to assess the general utility of toxicogenomics in deriving a POD by comparing the toxicogenomic PODs to the relevant apical endpoint PODs. Similar analyses that have combined data from multiple tissues and species support that transcriptomic PODs are similar to those derived using conventional approaches [see (Thomas et al., 2013)]. Scrutiny of the similarity between apical and transcriptional PODs is essential as we move towards an era where toxicogenomics may be used to produce data rapidly for regulatory decision-making.

et al., 2017) transcriptomic studies. The fact that such downregulation is observed in human carcinoma samples suggests that this may be an adverse response within the carcinogenic MOA of AA that is relevant to humans. However, more studies are required to confirm this hypothesis.

6. Conclusions

Overall, this study provides further support that CS is involved in AA-mediated carcinogenesis in rodents. This study expands the number of cancer target tissues and species in which gene expression changes associated with CS are detectable following AA exposure (Recio et al., 2017; Chepelev et al., 2017). Furthermore, the effect on the CS pathway appears to be the only thing in common between the cancer target tissues of AA examined here and in our earlier reports in rats. AA-induced alteration in gene expression in the CS pathway is consistent with earlier reports demonstrating AA-induced neurotoxicity associated with the interaction of AA with calcium and cytoskeletal proteins. The involvement of CS perturbations as a KE in carcinogenesis is in agreement with the ability of calcium to contribute to various hallmarks of cancer. Our global transcriptomic analysis also provides mechanistic insight that will be useful in further understanding the role of CS in induced carcinogenesis in general. This extensive study encompassing exposure doses both above and below those causing cancer, multiple times points, two species and five tissues in total (including both cancer target and a non-target tissue) strongly suggests that analysis of calcium levels, associated signaling proteins (e.g., Mef2C and Ryr1), and potential cytoskeletal effects, should be the subject of future studies on AA toxicity. Finally, RNA-seq data from the mouse lung and Harderian (and from other AA cancer target tissues reported separately) provide transcriptomic PODs that are within 1–3 fold of PODs from 2-year cancer bioassays, supporting the utility of toxicogenomics in human health risk assessment, especially for data-poor compounds.

Acknowledgements

This work was supported by SNF SAS and Health Canada's Chemicals Management Plan (CMP). We thank ILS animal care, necropsy staff and Jeffrey Davis, study director for the in-life portion of this study. We are grateful to Dr. Ivy Moffat and Dr. Mike Wade for their helpful comments on this manuscript.

Appendix A. Supplementary data

Supplementary data related to this article can be found at <https://doi.org/10.1016/j.yrtph.2018.02.005>.

Transparency document

Transparency document related to this article can be found online at <https://doi.org/10.1016/j.yrtph.2018.02.005>.

References

- Albert, D.M., Frayer, W.C., Black, H.E., Massicotte, S.J., Sang, D.N., Soque, J., 1986. The harderian gland: its tumors and its relevance to humans. *Trans. Am. Ophthalmol. Soc.* 84, 321–341.
- Arocena, M., 2006. Effect of acrylamide on the cytoskeleton and apoptosis of bovine lens epithelial cells. *Cell Biol. Int.* 30, 1007–1012.
- Beebe, S.P., 1904. The chemistry of malignant growth. II. The inorganic constituents of tumors. *Am. J. Physiol.* 12, 167–172.
- Beland, F.A., Mellick, P.W., Olson, G.R., Mendoza, M.C.B., Marques, M.M., Doerge, D.R., 2013. Carcinogenicity of acrylamide in B6C3F1 mice and F344/N rats from a 2-year drinking water exposure. *Food Chem. Toxicol.* 51, 149–159.
- Bidaux, G., Flourakis, M., Thebault, S., Zholos, A., Beck, B., Gkika, D., Roudbaraki, M., Bonnal, J.L., Mauroy, B., Shuba, Y., Skryma, R., Prevarskaya, N., 2007. Prostate cell differentiation status determines transient receptor potential melastatin member 8 channel subcellular localization and function. *J. Clin. Invest.* 117, 1647–1657.
- Bowyer, J.F., Latendresse, J.R., Delongchamp, R.R., Muskhelishvili, L., Warbritton, A.R., Thomas, M., Tareke, E., McDaniel, L.P., Doerge, D.R., 2008. The effects of subchronic acrylamide exposure on gene expression, neurochemistry, hormones, and histopathology in the hypothalamus-pituitary-thyroid axis of male Fischer 344 rats. *Toxicol. Appl. Pharmacol.* 230, 208–215.
- Carruthers, C., Sunzef, V., 1944. The role of calcium in carcinogenesis. *Science* 99, 245–247.

- Cerutti, J.M., Oler, G., Delcelo, R., Gerardt, R., Michaluart Jr., P., de Souza, S.J., Galante, P.A., Huang, P., Riggins, G.J., 2011. PVALB, a new Hurthle adenoma diagnostic marker identified through gene expression. *J. Clin. Endocrinol. Metab.* 96, E151–E160.
- Chemaly, E.R., Troncone, L., Lebeche, D., 2018. SERCA control of cell death and survival. *Cell Calcium* 69, 46–61.
- Chepelev, N.L., Moffat, I.D., Bowers, W.J., Yauk, C.L., 2015a. Neurotoxicity may be an overlooked consequence of benzo[a]pyrene exposure that is relevant to human health risk assessment. *Mutat. Res. Rev. Mutat. Res.* 764, 64–89.
- Chepelev, N., Moffat, I., Labib, S., Bourdon, J., Williams, A., Kuo, B., Buick, J., Lemieux, F., Malik, A., Halappanavar, S., Yauk, C., 2015b. Integrating toxicogenomics into human health risk assessment: lessons learned from the benzo[a]pyrene case study. *Crit. Rev. Toxicol.* 45, 44–52.
- Chepelev, N.L., Gagne, R., Maynor, T., Kuo, B., Hobbs, C.A., Recio, L., Yauk, C.L., 2017. Transcriptional profiling of male F344 rats suggests the involvement of calcium signaling in the mode of action of acrylamide-induced thyroid cancer. *Food Chem. Toxicol.*
- Clewell, H.J., Thomas, R.S., Kenyon, E.M., Hughes, M.F., Adair, B.M., Gentry, P.R., Yager, J.W., 2011. Concentration- and time-dependent genomic changes in the mouse urinary bladder following exposure to arsenate in drinking water for up to 12 weeks. *Toxicol. Sci.* 123, 421–432.
- Clowes, G.H.A., Frisbie, W.S., 1905. On the relationship between the rate of growth, age and potassium and calcium content of mouse tumors (Adeno-Carcinoma, Jensen). *Am. J. Physiol.* 14, 173–192.
- Cohen, S.M., Arnold, L.L., Beck, B.D., Lewis, A.S., Eldan, M., 2013. Evaluation of the carcinogenicity of inorganic arsenic. *Crit. Rev. Toxicol.* 43, 711–752.
- Dang, D., Rao, R., 2016. Calcium-ATPases: gene disorders and dysregulation in cancer. *Biochim. Biophys. Acta* 1863, 1344–1350.
- Dobin, A., Davis, C.A., Schlesinger, F., Drenkow, J., Zaleski, C., Jha, S., Batut, P., Chaisson, M., Gingeras, T.R., 2013. STAR: ultrafast universal RNA-seq aligner. *Bioinformatics* 29, 15–21.
- Dobrovolsky, V.N., Pacheco-Martinez, M.M., McDaniel, L.P., Pearce, M.G., Ding, W., 2016. In vivo genotoxicity assessment of acrylamide and glycidyl methacrylate. *Food Chem. Toxicol.* 87, 120–127.
- Doerge, D.R., Young, J.F., McDaniel, L.P., Twaddle, N.C., Churchwell, M.I., 2005a. Toxicokinetics of acrylamide and glycidamide in B6C3F1 mice. *Toxicol. Appl. Pharmacol.* 202, 258–267.
- Doerge, D.R., Young, J.F., McDaniel, L.P., Twaddle, N.C., Churchwell, M.I., 2005b. Toxicokinetics of acrylamide and glycidamide in Fischer 344 rats. *Toxicol. Appl. Pharmacol.* 208, 199–209.
- Dourson, M., Hertzberg, R., Allen, B., Haber, L., Parker, A., Kroner, O., Maier, A., Kohrman, M., 2008. Evidence-based dose-response assessment for thyroid tumorigenesis from acrylamide. *Regul. Toxicol. Pharmacol.* 52, 264–289.
- Durham, H.D., Pena, S.D.J., Carpenter, S., 1983. The neurotoxins 2,5-hexanedione and acrylamide promote aggregation of intermediate filaments in cultured fibroblasts. *Muscle Nerve* 6, 631–637.
- Eckert, B.S., 1985. Alteration of intermediate filament distribution in PtK1 cells by acrylamide. *Eur. J. Cell Biol.* 37, 169–174.
- Edgar, R., Domrachev, M., Lash, A.E., 2002. Gene Expression Omnibus: NCBI gene expression and hybridization array data repository. *Nucleic Acids Res.* 30, 207–210.
- EFSA Panel on Contaminants in the Food Chain (CONTAM), 2015. Scientific Opinion on acrylamide in food. *EFSA J.* 13, 1404/n/a.
- FAO/WHO (Joint FAO/WHO Expert Committee on Food Additives), 2011. Seventy-second report of the joint FAO/WHO expert committee on food additives (rome, 16–25 february 2010). Evaluation of certain food contaminants. WHO Tech. Rep. Ser. 959, 115.
- Farmahin, R., Williams, A., Kuo, B., Chepelev, N.L., Thomas, R.S., Barton-Maclaren, T.S., Curran, I.H., Nong, A., Wade, M.G., Yauk, C.L., 2016. Recommended approaches in the application of toxicogenomics to derive points of departure for chemical risk assessment. *Arch. Toxicol.* 1–21.
- Fennell, T.R., Snyder, R., Hansen, B., Friedman, M., 2015. Dosimetry of acrylamide and glycidamide over the lifespan in a 2-year bioassay of acrylamide in wistar han rats. *Toxicol. Sci.* 146, 386–394.
- Friedman, M.A., Dulak, L.H., Stedham, M.A., 1995. A lifetime oncogenicity study in rats with acrylamide. *Fund. Appl. Toxicol.* 27, 95–105.
- Friedman, M.A., Zeiger, E., Marroni, D.E., Sickles, D.W., 2008. Inhibition of rat testicular nuclear kinesins (krp2; KIFC5A) by acrylamide as a basis for establishing a genotoxicity threshold. *J. Agric. Food Chem.* 56, 6024–6030.
- Gall, L., De Smedt, V., Ruffini, S., 1992. Co-expression of cytokeratins and vimentin in sheep cumulus-oocyte complexes. Alteration of intermediate filament distribution by acrylamide: granulosa cells/vimentin/cytokeratin/acrylamide/maturation. *Dev. Growth Differ.* 34, 579–587.
- Ghanayem, B.I., McDaniel, L.P., Churchwell, M.I., Twaddle, N.C., Snyder, R., Fennell, T.R., Doerge, D.R., 2005a. Role of CYP2E1 in the epoxidation of acrylamide to glycidamide and formation of DNA and hemoglobin adducts. *Toxicol. Sci.* 88, 311–318.
- Ghanayem, B.I., Witt, K.L., Kissling, G.E., Tice, R.R., Recio, L., 2005b. Absence of acrylamide-induced genotoxicity in CYP2E1-null mice: evidence consistent with a glycidamide-mediated effect. *Mutat. Res. Fund Mol. Mech. Mutagen* 578, 284–297.
- Hartley, S.W., Mullikin, J.C., 2015. QORTs: a comprehensive toolset for quality control and data processing of RNA-Seq experiments. *BMC Bioinf.* 16.
- Hobbs, C.A., Davis, J., Shepard, K., Chepelev, N., Friedman, M., Marroni, D., Recio, L., 2016. Differential genotoxicity of acrylamide in the micronucleus and Pig-a gene mutation assays in F344 rats and B6C3F1 mice. *Mutagenesis* 31, 617–626.
- Hoth, M., 2016. CRAC channels, calcium, and cancer in light of the driver and passenger concept. *Biochim. Biophys. Acta* 1863, 1408–1417.
- Institute for Laboratory Animal Research, 1996. Guide for the Care and Use of Laboratory Animals. The National Academies Press, Washington, D.C.
- Johnson, K.A., Gorzinski, S.J., Bodner, K.M., Campbell, R.A., Wolf, C.H., Friedman, M.A., Mast, R.W., 1986. Chronic toxicity and oncogenicity study on acrylamide incorporated in the drinking water of Fischer 344 rats. *Toxicol. Appl. Pharmacol.* 85, 154–168.
- Katen, A.L., Stanger, S.J., Anderson, A.L., Nixon, B., Roman, S.D., 2016. Chronic acrylamide exposure in male mice induces DNA damage to spermatozoa; Potential for amelioration by resveratrol. *Reprod. Toxicol.* 63, 1–12.
- Kuehner, S., Holzmann, K., Speit, G., 2013. Characterization of formaldehyde's genotoxic mode of action by gene expression analysis in TK6 cells. *Arch. Toxicol.* 87, 1999–2012.
- Kuo, B., Francina Webster, A., Thomas, R.S., Yauk, C.L., 2015. BMDEExpress Data Viewer - a visualization tool to analyze BMDEExpress datasets. *J. Appl. Toxicol.* 36, 1048–1059.
- Langmead, B., Salzberg, S.L., 2012. Fast gapped-read alignment with Bowtie 2. *Nat. Methods* 9, 357–359.
- Lapadula, D.M., Bowe, M., Carrington, C.D., Dulak, L., Friedman, M., Abou-Donia, M.B., 1989. In vitro binding of [¹⁴C]acrylamide to neurofilament and microtubule proteins of rats. *Brain Res.* 481, 157–161.
- LoPachin, R.M., Gavin, T., 2012. Molecular mechanism of acrylamide neurotoxicity: lessons learned from organic chemistry. *Environ. Health Perspect.* 120, 1650–1657.
- Marchi, S., Pinto, P., 2016. Alterations of calcium homeostasis in cancer cells. *Curr. Opin. Pharmacol.* 29, 1–6.
- Maronpot, R.R., Thoolen, R.J.M.M., Hansen, B., 2015. Two-year carcinogenicity study of acrylamide in Wistar Han rats with in utero exposure. *Exp. Toxicol. Pathol.* 67, 189–195.
- Martins, C., Oliveira, N.G., Pingarilho, M., Gamboa da Costa, G., Martins, V., Marques, M.M., Beland, F.A., Churchwell, M.I., Doerge, D.R., Rueff, J., Gaspar, J.F., 2007. Cytogenetic damage induced by acrylamide and glycidamide in mammalian cells: correlation with specific glycidamide-DNA adducts. *Toxicol. Sci.* 95, 383–390.
- McDougal, J.N., Jones, K.L., Fatuyi, B., Gray, K.J., Blount, B.C., Valentin-Blasini, L., Fisher, J.W., 2011. The effects of perchlorate on thyroidal gene expression are different from the effects of iodide deficiency. *J. Toxicol. Environ. Health Part A Curr. Iss.* 74, 917–926.
- Meek, M.E., Palermo, C.M., Bachman, A.N., North, C.M., Jeffrey Lewis, R., 2014. Mode of action human relevance (species concordance) framework: evolution of the Bradford Hill considerations and comparative analysis of weight of evidence. *J. Appl. Toxicol.* 34, 595–606.
- Mei, N., Hu, J., Churchwell, M.I., Guo, L., Moore, M.M., Doerge, D.R., Chen, T., 2008. Genotoxic effects of acrylamide and glycidamide in mouse lymphoma cells. *Food Chem. Toxicol.* 46, 628–636.
- Mei, N., McDaniel, L.P., Dobrovolsky, V.N., Guo, X., Shaddock, J.G., Mittelstaedt, R.A., Azuma, M., Shelton, S.D., McGarrity, L.J., Doerge, D.R., Heflich, R.H., 2010. The genotoxicity of acrylamide and glycidamide in big blue rats. *Toxicol. Sci.* 115, 412–421.
- Miller, K., 1977. Calcium and cancer. *Med. Hypotheses* 3, 263–264.
- Moffat, I., Chepelev, N., Labib, S., Bourdon-Lacombe, J., Kuo, B., Buick, J.K., Lemieux, F., Williams, A., Halappanavar, S., Malik, A., Luijten, M., Aubrecht, J., Hyduke, D.R., Fornace, A.J.J., Swartz, C.D., Recio, L., Yauk, C.L., 2015. Comparison of toxicogenomics and traditional approaches to inform mode of action and points of departure in human health risk assessment of benzo[a]pyrene in drinking water. *Crit. Rev. Toxicol.* 45, 1–43.
- Monteith, G.R., Prevarskaya, N., Roberts-Thomson, S.J., 2017. The calcium-cancer signalling nexus. *Nat. Rev. Canc.* 17, 367–380.
- Novak, R.F., Woodcroft, K.J., 2000. The alcohol-inducible form of cytochrome P450 (CYP 2E1): role in toxicology and regulation of expression. *Arch. Pharm. Res. (Seoul)* 23, 267–282.
- Okamoto, S., Nakamura, T., Cieplak, P., Chan, S.F., Kalashnikova, E., Liao, L., Saleem, S., Han, X., Clemente, A., Nutter, A., Sances, S., Brechtel, C., Haus, D., Haun, F., Sanz-Blasco, S., Huang, X., Li, H., Zaremba, J.D., Cui, J., Gu, Z., Nikzad, R., Harrop, A., McKercher, S.R., Godzik, A., Yates 3rd, J.R., Lipton, S.A., 2014. S-nitrosylation-mediated redox transcriptional switch modulates neurogenesis and neuronal cell death. *Cell Rep.* 8, 217–228.
- Reagan, K.E., Wilmarth, K.R., Friedman, M., Abou-Donia, M.B., 1994. Acrylamide increases in vitro calcium and calmodulin-dependent kinase-mediated phosphorylation of rat brain and spinal cord neurofilament proteins. *Neurochem. Int.* 25, 133–143.
- Recio, L., Friedman, M., Marroni, D., Maynor, T., Chepelev, N.L., 2017. Impact of acrylamide on calcium signaling and cytoskeletal filaments in testes from F344 rat. *Int. J. Toxicol.* 36, 124–132.
- Robinson, M.D., Oshlack, A., 2010. A scaling normalization method for differential expression analysis of RNA-seq data. *Genome Biol.* 11, R25–2010-11-3-r25. Epub 2010 Mar 2.
- Robinson, M.D., McCarthy, D.J., Smyth, G.K., 2010. edgeR: a Bioconductor package for differential expression analysis of digital gene expression data. *Bioinformatics* 26, 139–140.
- Sager, P.R., 1989. Cytoskeletal effects of acrylamide and 2,5-hexanedione: selective aggregation of vimentin filaments. *Toxicol. Appl. Pharmacol.* 97, 141–155.
- Shipp, A., Lawrence, G., Gentry, R., McDonald, T., Bartow, H., Bounds, J., Macdonald, N., Clewell, H., Allen, B., Van Landingham, C., 2006. Acrylamide: review of toxicity data and dose-response analyses for cancer and noncancer effects. *Crit. Rev. Toxicol.* 36, 481–608.
- Sickles, D.W., Welter, D.A., Friedman, M.A., 1995. Acrylamide arrests mitosis and prevents chromosome migration in the absence of changes in spindle microtubules. *J. Toxicol. Environ. Health* 44, 73–86.
- Sickles, D.W., Brady, S.T., Testino, A., Friedman, M.A., Wrenn, R.W., 1996. Direct effect of the neurotoxicant acrylamide on kinesin-based microtubule motility. *J. Neurosci. Res.* 46, 7–17.
- Sickles, D.W., Stone, J.D., Friedman, M.A., 2002. Fast axonal transport: a site of acrylamide neurotoxicity?. *Neurotoxicology* 23, 223–251.
- Sickles, D.W., Sperry, A.O., Testino, A., Friedman, M., 2007. Acrylamide effects on kinesin-related proteins of the mitotic/meiotic spindle. *Toxicol. Appl. Pharmacol.* 222, 111–121.

- Slob, W., 2017. A general theory of effect size, and its consequences for defining the benchmark response (BMR) for continuous endpoints. *Crit. Rev. Toxicol.* 47, 342–351.
- Smith, M.T., Guyton, K.Z., Gibbons, C.F., Fritz, J.M., Portier, C.J., Rusyn, I., DeMarini, D.M., Caldwell, J.C., Kavlock, R.J., Lambert, P.F., Hecht, S.S., Bucher, J.R., Stewart, B.W., Baan, R.A., Coglian, V.J., Straif, K., 2016. Key characteristics of carcinogens as a basis for organizing data on mechanisms of carcinogenesis. *Environ. Health Perspect.* 124, 713–721.
- Stewart, T.A., Yapa, K.T.D.S., Monteith, G.R., 2015. Altered calcium signaling in cancer cells. *Biochim. Biophys. Acta Biomembr.* 1848, 2502–2511.
- Sun, Q.A., Wang, B., Miyagi, M., Hess, D.T., Stamler, J.S., 2013. Oxygen-coupled redox regulation of the skeletal muscle ryanodine receptor/Ca²⁺ release channel (RyR1): sites and nature of oxidative modification. *J. Biol. Chem.* 288, 22961–22971.
- Thomas, R.S., Clewell III, H.J., Allen, B.C., Wesselkamper, S.C., Wang, N.C.Y., Lambert, J.C., Hess-Wilson, J.K., Zhao, Q.J., Andersen, M.E., 2011. Application of transcriptional benchmark dose values in quantitative cancer and noncancer risk assessment. *Toxicol. Sci.* 120, 194–205.
- Thomas, R.S., Philbert, M.A., Auerbach, S.S., Wetmore, B.A., Devito, M.J., Cote, I., Rowlands, J.C., Whelan, M.P., Hays, S.M., Andersen, M.E., Meek, M.E.B., Reiter, L.W., Lambert, J.C., Clewell, H.J., Stephens, M.L., Zhao, Q.J., Wesselkamper, S.C., Flowers, L., Carney, E.W., Pastoor, T.P., Petersen, D.D., Yauk, C.L., Nong, A., 2013. Incorporating new technologies into toxicity testing and risk assessment: moving from 21st century vision to a data-driven framework. *Toxicol. Sci.* 136, 4–18.
- US Environmental Protection Agency (EPA), 2010. Toxicological Review of Acrylamide. 2015, 1–295, Available at: <http://www.epa.gov/iris/toxreviews/0286tr.pdf>.
- Watzek, N., Bohm, N., Feld, J., Scherbl, D., Berger, F., Merz, K.H., Lampen, A., Reemtsma, T., Tannenbaum, S.R., Skipper, P.L., Baum, M., Richling, E., Eisenbrand, G., 2012. N7-glycidamide-guanine DNA adduct formation by orally ingested acrylamide in rats: a dose-response study encompassing human diet-related exposure levels. *Chem. Res. Toxicol.* 25, 381–390.
- Yang, L., Allen, B.C., Thomas, R.S., 2007. BMDExpress: a software tool for the benchmark dose analyses of genomic data. *BMC Genom.* 8, 387.
- Zeiger, E., Recio, L., Fennell, T.R., Haseman, J.K., Snyder, R.W., Friedman, M., 2009. Investigation of the low-dose response in the *in vivo* induction of micronuclei and adducts by acrylamide. *Toxicol. Sci.* 107, 247–257.